UNIVERSIDADE ESTADUAL PAULISTA
Faculdade de Engenharia
Campus de Bauru

FABIO ISAAC FERREIRA

CORRELATION BETWEEN ELECTROMECHANICAL IMPEDANCE AND SURFACE QUALITY OF GROUND WORKPIECES

BAURU

2020

FABIO ISAAC FERREIRA

CORRELATION BETWEEN ELECTROMECHANICAL IMPEDANCE AND SURFACE QUALITY OF GROUND WORKPIECES

A thesis presented to the Faculty of Engineering Bauru (FEB) in partial fulfillment of the requirements for the doctoral degree (Ph.D.) in the subject of Electrical Engineering.

Advisor: Dr. Paulo Roberto de Aguiar

Ferreira, Fábio Isaac.
Correlation between electromechanical impedance and surface quality of ground workpieces / Fábio Isaac Ferreira, 2020
83 f. : il.

Orientador: Paulo Roberto de Aguiar

Tese (Doutorado)-Universidade Estadual Paulista. Faculdade de Engenharia, Bauru, 2020

1. Grinding. 2. Electromechanical impedance. 3. Piezoelectric transducer. 4. Structural health monitoring. 5. Surface Quality. I. Universidade Estadual Paulista. Faculdade de Engenharia. II. Título.

UNIVERSIDADE ESTADUAL PAULISTA

Câmpus de Bauru

ATA DA DEFESA PÚBLICA DA TESE DE DOUTORADO DE FÁBIO ISAAC FERREIRA, DISCENTE DO PROGRAMA DE PÓS-GRADUAÇÃO EM ENGENHARIA ELÉTRICA, DA FACULDADE DE ENGENHARIA - CÂMPUS DE BAURU.

Aos 03 dias do mês de agosto do ano de 2020, às 14:00 horas, no(a) Via sistemas de videoconferência e outras ferramentas para comunicação a distância, reuniu-se a Comissão Examinadora da Defesa Pública, composta pelos seguintes membros: Prof. Dr. PAULO ROBERTO DE AGUIAR - Orientador(a) do(a) Departamento de Engenharia Elétrica / Faculdade de Engenharia de Bauru - UNESP, Prof. Dr. FABRICIO GUIMARÃES BAPTISTA do(a) Departamento de Engenharia Elétrica / Faculdade de Engenharia de Bauru - UNESP, Prof. Dr. ROSEMAR BATISTA DA SILVA do(a) Faculdade de Engenharia Mecânica / Universidade Federal de Uberlândia, Prof. Dr. BRUNO ALBUQUERQUE DE CASTRO do(a) Departamento de Mecatrônica / FATEC - Faculdade de Tecnologia de Garça, Prof. Dr. BRENO ORTEGA FERNANDEZ do(a) Departamento de Engenharia Elétrica / Centro Universitário de Lins - UNILINS, sob a presidência do primeiro, a fim de proceder a arguição pública da TESE DE DOUTORADO de FÁBIO ISAAC FERREIRA, intitulada **CORRELATION BETWEEN ELECTROMECHANICAL IMPEDANCE AND SURFACE QUALITY OF GROUND WORKPIECES**. Após a exposição, o discente foi arguido oralmente pelos membros da Comissão Examinadora, tendo recebido o conceito final: Aprovado. Nada mais havendo, foi lavrada a presente ata, que após lida e aprovada, foi assinada pelos membros da Comissão Examinadora.

Prof. Dr. PAULO ROBERTO DE AGUIAR

Prof. Dr. FABRICIO GUIMARÃES BAPTISTA p/

Prof. Dr. ROSEMAR BATISTA DA SILVA p/

Prof. Dr. BRUNO ALBUQUERQUE DE CASTRO p/

Prof. Dr. BRENO ORTEGA FERNANDEZ p/

This research work is wholeheartedly dedicated to my beloved parents, who have been my source of inspiration and gave me strength when I thought of giving up, who continually provide their spiritual, moral, and emotional support.

ACKNOWLEDGMENTS

The researcher would like to give thanks to all the persons that somehow contributed with this study.

To God for giving me the inspiration and strength to conduct this study.

To my entire family, specially to my mother Rosa, father Antonio, sister Caroline, brother Alexandre, and grandmother Lidia, for their moral and emotional support during this period.

To my advisor in Brazil, Dr. Paulo R. de Aguiar, who guided and helped me to make the study a well-done achievement, sharing his words of advice and encouragement to finish it.

To my advisor in the USA, Dr. Mark J. Jackson, for accepting me as a Research Scholar at Kansas State University, Polytechnic campus, sharing his experience and showing me different points of view.

To professors Dr. Rosemar B. da Silva, Dr. Fabricio G. Baptista, and Eduardo C. Bianchi, who contributed to make this study happen.

To all my friends and classmates who have been with me during this journey and showed me how important is the value of friendship.

To Sao Paulo State University (Unesp), which provided facilities to the electromechanical impedance measurements, to Federal University of Uberlandia (UFU), where surface grinding has been performed, and to Kansas State University Polytechnic campus (K-State), where cylindrical grinding and electromechanical impedance measurements have been conducted.

To the Blaser Swisslube, Villares Metals, Saint Gobain Abrasives for the donation of the coolant, workpiece material, and grinding wheel, respectively, and to the Advanced Manufacturing Institute (AMI) to provide the data acquisition board.

This study was financed in part by the Coordenação de Aperfeiçoamento de Pessoal de Nível Superior – Brasil (CAPES) – Finance Code PDSE 88881.190384/2018-01.

RESUMO

A retificação é um processo de manufatura de extrema importância para a produção de partes de alta precisão e para garantir sua qualidade superficial. Medições elétricas desempenham um importante papel em métodos de monitoramento indireto, os quais garantem a eficiência do processo. No entanto, métodos tradicionais utilizam sensores de alto custo e requerem esforços computacionais expressivos. Este estudo discute correlações entre a técnica da Impedância Eletromecânica (EMI) e parâmetros mecânicos e elétricos do processo da retificação. A técnica EMI aplicada na retificação é inédita e tem a vantagem de empregar equipamentos de baixo custo, que requerem um sistema de monitoramento mais simples, quando comparado com as técnicas tradicionalmente utilizadas. Este trabalho propõe apresentar o potencial desta técnica, a qual poderia substituir satisfatoriamente os métodos tradicionais. Dois conjuntos de testes laboratoriais foram realizados independentemente para estudar a correlação entre medições EMI e parâmetros do processo. O primeiro conjunto de testes estudou a técnica EMI aplicada na retificação plana tangencial, enquanto o segundo, na retificação cilíndrica de mergulho. Em ambos os testes, experimentos foram realizados em um ambiente controlado para isolar as variáveis de interesse e as medidas EMI foram investigadas para diversas bandas de frequências. Para a retificação plana, fortes correlações entre EMI e espessura equivalente de corte, rugosidade média, microdureza e sinais de potência foram encontradas. Para a retificação cilíndrica, correlação entre rugosidade média e os índices de dano foram obtidos. Esses resultados permitem inferir informações sobre o processo da retificação através do monitoramento indireto.

Palavras-chave: retificação, impedância eletromecânica, transdutor piezoelétricos, monitoramento da integridade estrutura, qualidade superficial.

ABSTRACT

Grinding is a machining process of utmost importance to produce high precision parts and guarantee surface quality. Several techniques have been studied throughout the years to improve the quality of workpieces manufactured by the grinding process. Electrical measurements play a key role during indirect monitoring methods which enhance the process efficiency due to the continuity of the operation by an on-line monitoring system. However, well-established methods, such as acoustic emission and vibration signals, employ high-cost sensors and require tough computational efforts. This study discusses correlations among Electromechanical Impedance (EMI) technique and mechanical and electrical parameters from grinding. The EMI technique applied in grinding is innovative and has the advantage of employing cheaper equipment and requiring a simpler monitoring system when compared to traditional techniques. This work aims to show the potential of that new technique, which can appropriately replace the traditional ones. To this end, two experimental tests sets were conducted independently to study the correlation between EMI measurements and parameters from the process. The first studied the EMI technique on surface grinding, while the second studied on cylindrical grinding. In both, tests were performed in a controlled environment to isolate the variables of interest and EMI was investigated for several frequency bands. For the surface grinding, strong correlations among EMI and equivalent chip thickness, roughness, and microhardness of the workpiece, as well as power signals were found out. The RMSD (root-mean-square deviation) index for the real part of the signature in the band 80-85 kHz showed a good correlation with roughness and power, while the CCDM (correlation coefficient deviation metric) index for the imaginary part of 50-55 kHz showed good correlation with microhardness. For the cylindrical grinding, the correlation between surface roughness and damage indices was studied and the best correlation was found to be with the CCDM index in the frequency band of 125-130 kHz. Those results allow the user to infer information about the grinding process through indirect monitoring.

Keywords: grinding, electromechanical impedance, piezoelectric transducer, structural health monitoring, surface quality.

LIST OF FIGURES

LIST OF TABLES

LIST OF ABBREVIATIONS

ADC – Analog-to-Digital Converter

a_d – Dressing Depth, µm

ae – Radial depth of Cut, µm

bw – Bandwidth, kHz

AE – Acoustic Emission

EMI – Electromechanical Impedance

C – Capacitance, F

CCDM – Correlation Coefficient Deviation Metric

DAQ – Data Acquisition

DFT – Discrete Fourier Transform

f – Frequency, Hz

FRF – Frequency Response Function

h_{eq} – Equivalent Chip Thickness, µm

MQL – Minimum Quantity Lubrication

PLB – Pencil-Lead-Break

PZT – Pb-(lead) Zirconate Titanate

q_s – Ratio of Grinding Wheel/Workspeed

Q'_w – Specific Removal Rate, mm^2/min

ρ - Pearson Correlation Coefficient

RMSD – Root-Mean-Square Deviation

R_a – Arithmetic Average Roughness, µm

R_t – Maximum difference of roughness between peak height and valley depth, µm

R_z – Arithmetic average of roughness between the highest peak and lowest valley in each sampling length, µm

SHM – Structural Health Monitoring

TCM – Tool Condition Monitoring

U_d – Overlap Ratio

USB – Universal Serial Bus

v_d – Dressing Speed, mm/s

v_f - Radial Feed Rate, mm/min

v_s – Cutting Speed, m/s

v_w – Workspeed, m/min

X_c – Capacitive Reactance, Ω

Z_1 – Impedance of the Healthy Structure, Ω

Z_2 – Impedance of the Damaged Structure, Ω

Z_E – Electrical Impedance, Ω

Z_S – Mechanical Impedance of the Structure, Ω

Z_T – Mechanical Impedance of the Piezoelectric, Ω

CONTENTS

1 INTRODUCTION

Grinding is one of the most important processes of the manufacturing chain. Parts which require tight dimensional tolerances or high surface quality must be ground to guarantee design requirements. Since grinding is one of the last processes of the chain, the parts have high added value and losses cause high economic impact (Da Conceição Junior *et al.*, 2018). However, grinding is one of the most complex machining operations because of several aspects, such as heat transfer between cutting tool and the workpiece, which can cause thermal damages (Vendrame *et al.*, 2018).

To appropriately control machining operations, monitoring of mechanical systems is widely employed by industries that seek automation and quality in their manufacturing chains. Such intelligence level in the machines is reached by smart systems that might be composed of data acquisition equipment, signal processing, computational intelligence, optimization algorithms, and/or general actuators, which can play a key role in the productivity and efficiency of production processes. Monitoring systems can be designed for different purposes, such as:

- detecting and classifying conditions and failures;
- estimating the current values for the parameters of interest to guarantee dimensional, shape, and quality requirements;
- predicting steps forward to understand the behavior of the process parameters or tool wear and lifetime;
- taking part in the decision-making process such as emergency signals for the process security, stops to replace tools, or to avoid failures.

In each situation, researches have proposed different systems and techniques to indirectly monitor the process, as will be mentioned in the next section. Those systems can be used to replace parameters measurements, which often require stops or even harm the parts, causing their losses (Boaron and Weingaertner, 2018). Consequently, reliable and non-destructive systems are desired to improve the efficiency of the operations, to decrease economical losses, to reduce idle time, and to guarantee the quality of production chain.

However, most of them propose solutions that use expensive equipment and transducers (Tinoco *et al.*, 2019), or that are still inefficient for generic configurations (Alexandre *et al.*, 2018). Systems that can effectively be employed in the field are scarce and expensive and most of them are still being tested. The challenge is to find a monitoring system which can be effectively employed on operations.

1.1 Objective

As mentioned before, several techniques and equipment have been studied to achieve better results in the processes, improving quality and productivity. However, most of them require expensive equipment, complex set-ups and high computational efforts. Therefore, the objective of the present study is to investigate the electromechanical impedance (EMI) technique, in which it will be employed a low-cost transducer, applied to surface and cylindrical grinding. This technique is innovative for grinding operation, especially for miniaturized parts, such as small camshafts, and showed promising to replace traditional methods in previous tests.

Correlations between EMI and grinding parameters were studied in a controlled environment to verify if that technique could be used to replace traditional methods. Such investigation aims at an indirect monitoring system to be developed in the next works which ensures superior surface quality of ground workpieces by using low-cost equipment. The objective of this work is to show that the technique presented here has the potential to replace the traditional expensive methods, such as acoustic emission.

1.2 Justification

The investigation about EMI measurements applied to the quality of the grinding process is innovative and shows a great potential to be an alternative to replace classical techniques, such as acoustic emission and vibration signals. The present study differs from Marchi *et al.* (2015) because they studied the burn only by visual inspection and they did not consider other important aspects related to workpiece surface integrity. Moreover, this study differs from Junior, D'addona, *et al.* (2018) because they started to investigate the EMI technique applied on the dressing operation. We have published part of the results presented here in Batista da Silva *et al.* (2018) and in Ferreira *et al.* (2019), in which EMI technique was employed in surface grinding under controlled environmental conditions. The study of correlations between EMI and input (equivalent chip thickness, workspeed, feed rate) and output (roughness, microhardness, power) grinding parameters is discussed in more details in the current research, that includes real and imaginary parts of the impedance for several frequency bands. Moreover, the camshaft grinder that was employed in the current study is used to grind miniaturized parts. Therefore, this study is important to understand the behavior of the EMI when applied to surface and cylindrical grinding and to verify feasibility of industrial employment.

2 LITERATURE SURVAY

In this chapter, a literature review is conducted about the key topics of the current research. In the first section, indirect monitoring systems and relevant findings will be presented, which shows advantages over the direct monitoring systems. In the second section, the electromechanical impedance (EMI) technique is described, which gives theoretical support for the method described in this work. In the third section, fundamentals of the grinding process are reviewed, since grinding is the background topic that has been chosen for testing EMI on machining operations.

2.1 MONITORING APPLIED ON MANUFACTURING OPERATIONS

One of the major subjects that has been studied by researchers is the tool condition monitoring (TCM). Monitoring systems can be employed on machining processes aiming, for instance, at the tool wear progress and any alteration on the surface of the workpiece (Nguyen *et al.*, 2019). Several recent monitoring works are focused on the tool and most of them employ electric sensors to indirectly monitor, which are responsible for collecting information from the process itself. Signal behavior is analyzed by using data processing techniques and the results are correlated to tool wear, conducting estimations or predicting its features.

Uekita and Takaya (2017) proposed a technique to identify chatter and transient vibration from drill degradation by using an accelerometer, short-time Fourier transform, and spectral kurtosis. They found that chatter appeared abruptly close to a target frequency band, which caused tool failure.

Klaic *et al.* (2018) investigated rock drill wear in the drilling process by using vibration signals and found features from the frequency domain, which allowed to classify tool wear level using an RBF NN (radial basis function neural network).

Alexandre *et al.* (2018) studied grinding wheel wear by using acoustic emission (AE) signals and fuzzy models. They found high effective diagnosis to characterize surface conditions for filtered signals in the frequency band 25-40 kHz, which have been used to calculate the ratio of power (ROP) statistical parameter.

Ferreira *et al.* (2018) performed estimation and prediction of dresser width in the dressing process by AE emission signals and artificial neural networks (ANN) and found a system able to predict the next value of the dresser width by processing the AE signals calculated for the ROP parameter filtered for the frequency band of 32-34 kHz. That system can be used to readjust automatically the dressing parameters while avoiding stops.

Drouillet *et al.* (2016) demonstrated prediction of remaining useful life (RUL) of the tools, which was measured in minutes, based on milling tests by using power sensor and a curve fitting method of ANNs. They affirmed that their method is computationally inexpensive and took just about 0.5 seconds on an Intel i7 processor, providing a mean error of about 1 minute.

Some other relevant research works about TCM are mentioned as follows: grinding (Wegener *et al.*, 2011; Bhuiyan *et al.*, 2016; Arun *et al.*, 2018; Tanaka and Koshy, 2018); dressing operation (Martins *et al.*, 2014; Miranda *et al.*, 2015; Moia *et al.*, 2015; D'Addona *et al.*, 2016; da Conceição Junior *et al.*, 2018; Junior, D'addona, *et al.*, 2018; Junior, D'Addona, *et al.*, 2018); turning (Scheffer *et al.*, 2003; Hase *et al.*, 2014; Balsamo *et al.*, 2016; Bhuiyan *et al.*, 2016; Hocheng *et al.*, 2018); drilling (Klaic, Staroveski and Udiljak, 2014; Patra *et al.*, 2017; Caggiano *et al.*, 2018; Dong Wang *et al.*, 2019); and milling (Dai and Zhu, 2018; Zhang *et al.*, 2018; Alhadeff *et al.*, 2019; Hesser and Markert, 2019). Teti *et al.* (2010) describe several types of monitoring for the machining operations in their keynote paper presented in reference.

Manufacturing operations are vulnerable to various kind of failures given by factors such as: operational errors, low quality or worn tools, misalignment, incorrect parameters, thermal damages, uncalibrated instruments, etc. Such mistakes directly impact on the quality of the manufactured products, resulting in rework, or even disposal and, consequently, economical losses. Therefore, some research works focus on the quality of the product, trying to avoid failures and reaching minimum requirements. For example, in grinding, which was used as background for the technique studied in the present study, several works studied monitoring techniques to guarantee the requirements of dimensional and geometric tolerances without compromising surface integrity of the component.

Dias *et al.* (2016) conducted experiments on centerless grinding to investigate the correlation between AE signals and features of the workpiece, such as surface roughness R_z, roundness and cylindricity. They found that the lowest values for cylindricity and surface roughness, in dressing operation, was in the frequency range of 8,457-10,440 Hz, and roundness occurred in the frequency range of 7,122-7,257 Hz.

Studies about grinding burn are also recurrent in the scientific community and some recent papers employ different techniques, cited as follows: Barkhausen noise test (Neslušan *et al.*, 2017; Thanedar *et al.*, 2017); AE signal (Wang *et al.*, 2001; Aguiar, Bianchi and Canarim, 2012; Yang and Yu, 2012, 2013; Neto *et al.*, 2014; Yang *et al.*, 2014); vibration signals (Neto *et al.*, 2014); power signals (Aguiar, Dotto and Bianchi, 2005; Malkin and Guo, 2007); and electromechanical impedance measurement (Marchi *et al.*, 2015; Batista da Silva *et al.*, 2018). He *et al.* (2019) provided a description about different methods for detecting burn.

2.2 ELECTROMECHANICAL IMPEDANCE (EMI) TECHNIQUE

Structural health monitoring (SHM) systems are extensively deployed for monitoring damage in civil infrastructures, such as bridges and buildings (Sahni, Cao and Liu, 2018). For the purposes of the present work, structural damage will be defined as any state that differs from the state considered intact. The objective of SHM systems are to provide a high degree of security and to reduce costs of maintenance (Baptista and Filho, 2009). Several techniques can be employed to develop SHM systems, but the electromechanical impedance (EMI) technique has the virtue of using piezoelectric ceramics, such as compact, thin and low-cost piezoelectric diaphragms, PZTs (Pb-(lead) Zirconate Titanate) (Baptista and Filho, 2011). The piezoelectric effect occurs in materials that generate a voltage output as an electric dipole when they are under tensile stress. The reverse behavior also occurs, i.e., a mechanical deformation is generated when an electrical voltage is applied to the terminals of the piezoelectric material. For this reason, piezoelectric materials can be employed as sensors or actuators (Castro *et al.*, 2016).

The main concept of the EMI technique is to attach the transducer to the structure and, due to the piezoelectric effect, to observe the relationship between mechanical features of the structure and the electrical impedance of the transducer. Therefore, changes in the structure directly impact the impedance measurements.

Baptista and Filho (2009) proposed an impedance-based system using low-cost PZTs connected to a data acquisition (DAQ) device, which is conducted by the software LabVIEW, as shown in Figure 1. This system and their software are used to collect EMI signals, in which the PZT diaphragm is excited by an external voltage chirp signal made from the software throughout a wide frequency range and the response signal is simultaneously collected by the PZT and recorded by a computer. The response signal is digitally processed, through the discrete Fourier transform, to find the frequency-time domain, and the electromechanical impedance is calculated from the voltage signal. Baptista and Filho (2009) also presented the calibration signal, which is performed between the signal pattern generated by software *x[n]* and the signal that reaches the auxiliary circuit *x(t)*.

Figure 1 – Schematic of the method to conduct EMI the measurements

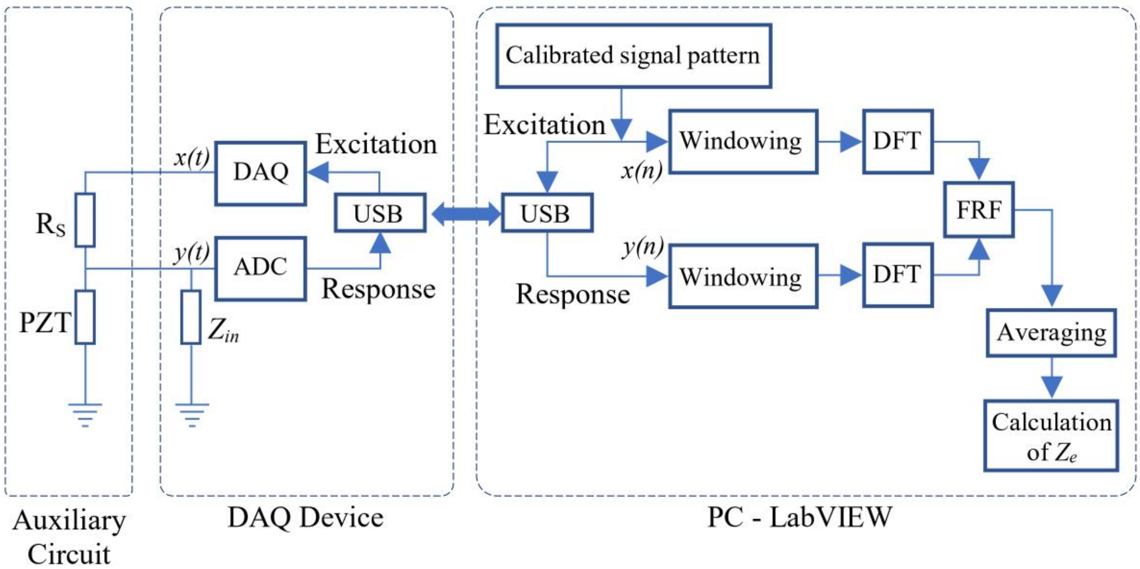

Source: Adapted from Baptista and Filho (2009)

According to Campeiro, da Silveira and Baptista (2018), external vibrations of low frequency can cause variations of the impedance signatures at higher frequencies. However, they stated that the effects of those disturbances can be attenuated by increasing the excitation level. According to Freitas et al., the mechanical impedance of the structure (Z_S) is related to the electrical impedance ($Z_D(\omega)$) measured in the terminals of the piezoelectric diaphragm, as shown in (1) (De Freitas *et al.*, 2017).

$$Z_D(\omega) = \frac{1}{j\omega C_0} \| \left\{ \left(\frac{2s_{11}^E}{\pi \phi_P d_{31}} \right)^2 \times \left[Z_{P2} + \frac{1}{2} \left(Z_{P1} + Z_{B1} + \frac{Z_{B2}(Z_{B1} + Z_S)}{Z_{B1} + Z_{B2} + Z_S} \right) \right] \right\} \quad (1)$$

In which:

ω: angular frequency,

j: imaginary number,

C_0: static capacitance of the piezoelectric diaphragm,

s_{11}^E: elastic compliance under a constant electric field,

ϕ_P: diameter of the piezoelectric element,

d_{31}: piezoelectric constant,

Z_{P1} and Z_{P2}: complex impedances for the piezoelectric element,

Z_{B1} and Z_{B2} are complex impedances for the brass disc,

||: parallel connection.

The complex impedances of the transducer are given by the (2) to (5).

$$Z_{P1} = jZ_P tan\left(\frac{k_P \phi_P}{2}\right) \quad (2)$$

$$Z_{P2} = -j \frac{Z_P}{\sin(k_P \phi_P)} \quad (3)$$

$$Z_{B1} = jZ_B \tan\left(\frac{k_B l_B}{2}\right) \quad (4)$$

$$Z_{B2} = -j \frac{Z_B}{\sin(k_B l_B)} \quad (5)$$

In which:

Z_P: mechanical impedance of the piezoelectric element,

Z_B: mechanical impedance of the brass disc,

l_B: brass path between the PZT ceramic and the monitored structure,

k_P and k_B: wave numbers, given by (6) and (7), respectively.

$$k_P = \omega\sqrt{s_{11}^E \rho_P} \tag{6}$$

$$k_B = \omega\sqrt{s_B \rho_B} \tag{7}$$

In which:

ρ_P: mass density of the PZT ceramic,

s_B: elastic compliance of the brass disc,

ρ_B: mass density of the brass disc.

EMI is analyzed in terms of the response signal frequencies (impedance signatures), i.e., how the EMI values (Ohm) change for different frequency values (Hz). When the structure being analyzed is considered in the intact state, that signature is defined as the baseline, but upon undergoing any damage (e.g. cracks, wear, corrosion, etc.), the amplitude or shape of the signature changes. Consequently, it is possible to differentiate between an intact and a damaged structure by comparing both signatures (Na and Lee, 2013) and the intensity of the damage can be quantified by means of the damage indices (Marchi *et al.*, 2015). According to da Silveira, Campeiro and Baptista (2017), the most common damage indices are the root-mean-square deviation (RMSD) and the correlation coefficient deviation metric (CCDM). The calculation for the RMSD index, which represents the Euclidean distance between the two signatures, is presented in (8):

$$RMSD = \sum_{\omega=\omega_I}^{\omega_F} \sqrt{\frac{\left[Re\left(Z_2(\omega)\right) - Re(Z_1(\omega))\right]^2}{Re(Z_1(\omega))^2}} \tag{8}$$

In which:

RMSD: index calculated for the frequency range from ω_I to ω_F,

$Re\left(Z_1(\omega)\right)$: real part of the baseline,

$Re\left(Z_2(\omega)\right)$: real part of the signature after damage.

Similarly, RMSD index can also be calculated from the module and imaginary part of the impedances. Previous works encourage using the real part of the impedance because it is less susceptible to temperature variations (Park *et al.*, 2003; Baptista *et al.*, 2013; da Silveira, Campeiro and Baptista, 2017). The CCDM index, which is related to the correlation coefficient between two signatures, can be calculated by (9):

$$CCDM = 1 - \frac{cov\left[Re\left(Z_1(\omega)\right), Re\left(Z_2(\omega)\right)\right]}{\sigma_1 \sigma_2} \tag{9}$$

In which:

cov: covariance between the real parts of Z_1 and Z_2 calculated for the frequency range from ω_I to ω_F,

σ_1 and σ_2: respective standard deviation of each signature.

In the same way as for RMSD, the CCDM index can be calculated from the module and imaginary part of the impedances.

2.3 THE GRINDING PROCESS

Four basic operations can be defined according to the movement of the equipment and the surface that is generated: peripheral surface grinding, peripheral cylindrical grinding, face surface grinding, and face cylindrical grinding (Marinescu *et al.*, 2007). In this work, the first and the second have been chosen to verify applicability of the EMI technique because the first produces flat surfaces, which is very common in several applications, and the second produces round parts, which is used to produce camshafts, crankshafts and bearings.

In the present section, relevant topics related to the grinding process will be reviewed. First, grinding technology will be explored, in which basic concepts from literature are presented to introduce the grinding operation. Second, definitions and equations about surface grinding are reviewed based on classical literature of manufacturing engineering. Third, the cylindrical grinding process is presented, which differs from surface grinding in the workpiece shape and, consequently, in grinding parameters. Fourth and last, surface quality of ground workpieces is discussed and the key parameters to measure it are presented.

2.3.1 Grinding technology

Grinding is widely employed in the industries that perform machining operations because it allows to obtain results with high quality and superior finish. The grinding process consists of a random integration of sliding, rubbing, and cutting stages by several abrasive grits disposed irregularly on the grinding wheel (Wang *et al.*, 2016).

Through the grinding process, it is possible to obtain a high dimensional and geometrical accuracy for the workpieces, as well as obtaining a great material removal rate. In this way, grinding can be applied to cutting manufacturing of hard and ultrahard materials (Akbari *et al.*, 2016). However, it is one of the most complex processes of the manufacturing chain because several factors impact on its performance, such as: grinding wheel, workpiece, machine, coolant, parameters, etc. (Tuan and Lee, 2008). Since grinding is one of the last stages of the manufacturing chain, failures must be avoided due to the high added value of each sample, which represents economical losses (Cearsolo *et al.*, 2016). Thus, to ensure that grinding presents the hoped results, it is of utmost importance that every parameter be studied and well-dimensioned, as well as operators be properly trained.

Another factor that strongly impacts on the quality of the grinding process is the temperature that is generated due to the friction between wheel and workpiece. So, it is important to provide an efficient and constant cooling system throughout the process. An alternative to traditional cooling system is the Minimum Quantity Lubrication (MQL), which attempts to dissipate the heat and consequently to decrease the temperature in the grinding zone, by using a mixture of compressed air and coolant in an optimized manner by spraying it. A cooling system is an essential component to increase quality of the ground surface and avoid thermal damages (Molaie, Akbari and Movahhedy, 2016). According to Malkin and Guo (2007), when temperature exceeds a defined threshold, about 400°C, thermal damages can occur to the ground workpiece, such as: burn, marks, phase transformation, increase or decrease of the hardness, tensile residual stress, and cracks. Therefore, the main purposes of employing cutting fluid is for cooling, removing chip, decreasing corrosion, cleaning the wheel, and mechanical lubrication (Molaie, Akbari and Movahhedy, 2016).

2.3.2 Surface grinding

Peripheral surface grinding is performed when flat surfaces are desired, involving linear movements. Five basic elements are used in the surface grinding: grinding machine, grinding wheel, workpiece, coolant, and the chip that is generated (Marinescu *et al.*, 2007).

The surface grinding leads to an interaction between abrasive wheel and workpiece which are dependent of some input parameters: material removal rate, cutting speed, workspeed, severity and spark out (KING and HAHN, 1992). The severity of the abrasive wheel also directly impacts on grinding and can be generated from the dressing operation (Ferreira *et al.*, 2018).

An important variable that must be considered in the grinding process is the radial depth of cut (*ae*). This parameter is defined by the depth of the abrasive wheel towards the workpiece that is ground. It represents the thickness of workpiece material that is removed at each pass of the wheel throughout the workpiece (Marinescu *et al.*, 2007). The radial depth of cut is set perpendicularly to direction of the wheel movement (DINIZ, MARCONDES and COPPINI, 2010). Radial depth of cut increase leads to cutting forces increase, which can cause deformation between wheel and sample and impair the quality of the ground surface (Linke, 2008).

The cutting speed is defined by a displacement of a dot on the cutting surface of the wheel by a unit of time variation. Such speed directly implies the wheel life because it affects its capacity of removing the abrasive grits and consequently the workpiece finishing (Malkin and Guo, 2008). According to GRAF (2004), the cutting speed can be calculated by (10).

$$v_s = \frac{\pi \cdot d_s \cdot n_s}{60000} \quad (10)$$

In which:

v_s: cutting speed, m/s,

d_s: external diameter of the grinding wheel, mm,

n_s: revolutions per minute of the grinding wheel, rpm.

When the grinding wheel is rotating at a higher speed, one single abrasive grit removes a little volume of chip due to the increase of frequency of contact with the workpiece. Then, the number of active grits is larger and the chip thickness that is removed is smaller, which decreases cutting forces, roughness, and wheel wear due to the lower effort of each grit. On the other hand, due to the contact intensity increase between grits and sample, temperature also increases which can cause thermal damage on the workpiece (Bianchi *et al.*, 1996).

The workspeed (v_w) represents the table speed in the surface grinding and is related to the impact that the abrasive grits cause to the workpiece. To quantify the metal removal rate of the workpiece per unit width of wheel contact, the specific removal rate (Q'_w or Q') is employed, as presented in (11) for surface grinding.

$$Q'_w = ae \cdot v_w \quad (11)$$

In which:

Q'_w or Q': specific removal rate, mm^2/min,

ae: radial depth of cut, mm,

v_w: workspeed, mm/min.

In general, low specific removal rate values are used to rubbing and ploughing, while high values are used to chip formation. However, when the workspeed is low and the radial depth of cut is high, the impacts of the grits upon the workpiece are small and the chip is long. In that situation, grits remain in contact with the workpiece for longer time, which causes greater wear of the abrasive grits. Cutting forces tend to increase throughout time due to the wear of sharp grits. Therefore, the wear of the wheel is smaller, considering that the abrasive grits remain for longer attached to the bonding, which reduces the grits losses (Marinescu *et al.*, 2007). When the workspeed is high and the radial depth of cut is low, the impact of the abrasive grits upon the workpiece are big and chips are short. The contact time between grit and workpiece and the number of active grits is lower, which cause great force on the grits during a short time. In this situation, the total cutting forces tend to stabilize by changing the grits constantly. Wheel wear tend to be larger than the first situation.

2.3.3 Cylindrical grinding

In the cylindrical grinding process, the grinding wheel rotates at high cutting speed ($v_s \geq 30$ m/s), similarly to peripheral surface grinding, and removes material from the workpiece surface due to frictional interactions. Marinescu et al. defined the cutting speed according to the revolutions per minute of the grinding wheel, which is also applicable for the cylindrical grinding process, since the cutting speed depends on the grinding wheel parameters (Marinescu *et al.*, 2007). The workpiece rotates at the workspeed (v_w), which is analogously calculated by (12).

$$v_w = \frac{\pi \cdot d_w \cdot n_w}{60000} \qquad (12)$$

In which:

v_w: workspeed, m/s,

d_w: external diameter of the workpiece, mm,

n_w: revolutions per minute of the workpiece, rpm.

According to Malkin and Guo (2008), the cutting speed is always much faster than the workspeed and the ratio can be quantified, as shown in (13).

$$q_s = \frac{v_s}{v_w} = \frac{d_s \cdot n_s}{d_w \cdot n_w} \qquad (13)$$

In which:

q_s: ratio of speeds,

v_s: cutting speed, m/s,

v_w: workspeed, m/s,

Values of q_s are used to point out the type of grinding that is being used, as follows (Macedo, 2012):

- Rough grinding: $60 < q_s < 90$
- Semi-finishing grinding: $q_s \cong 90$
- Finishing grinding: $90 < q_s < 120$

For cylindrical grinding, the specific removal rate (Q'_w or Q') is calculated from (14) (Marinescu *et al.*, 2007).

$$Q'_w = \pi \cdot d_w \cdot v_f \quad (14)$$

In which:

Q'_w or Q': specific removal rate, mm^3/mm-s,

d_w: external diameter of the workpiece, mm,

v_f: feed rate, mm/min.

Cylindrical plunge grinding, which is the processes commonly used to produce camshafts, crankshafts and bearings, requires roughness below 1.6 µm and international tolerance (IT) grade ranging from IT06 to IT03.

To perform an entire cycle of cylindrical plunge grinding, five stages can be defined (Hassui and Diniz, 2003). In the first one, the grinding wheel moves towards the workpiece at the feed adjusted to be used during cutting (v_f), but no contact and no chip removal is conducted. In the second, the contact between workpiece and grinding wheel begins and, because of the cutting forces, they both suffer elastic deformation. Hence, the feed decreases and the actual position of the contact between workpiece and grinding wheel delays. Third is the cutting phase, where feed increases back to the programmed value and chip is removed. Forth stage is when the spark-out is conducted by keeping the grinding wheel still with no feed during some seconds to recover the workpiece of the elastic deformation and to ensure it has the diameter that is desired. Finally, the grinding wheel is pulled back removing the contact.

2.3.4 Quality of ground surfaces

The generation of surfaces is obtained from abrasive finishing systems, in which the value and benefit of the part are specified in terms of the surface quality and how fast it can be generated (Oliveira *et al.*, 2009). The appropriate adjustment of grinding parameters is essential to ensure low surface roughness values, low dimensional deviations as well as to minimize damages. Surface quality takes into consideration two aspects: surface integrity and surface topography. The first is related to mechanical and metallurgical alterations to the surface layer generated during machining while the latter is associated to the geometry of machined surfaces, which is mainly represented by surface roughness (Malkin and Guo, 2008). It is known from the literature (Baumgart, Heizer and Wegener, 2018) that, during grinding of metals by using conventional abrasive grinding wheels, a great partition of the grinding energy is received by the workpiece in form of heat due to friction between the abrasive grits of the grinding wheel and the workpiece surface (Marinescu *et al.*, 2007), which can generate high temperatures on the grinding zone (Drazumeric, Badger and Krajnik, 2014).

Depending on the operating conditions, interaction between wheel and workpiece material can cause several types of thermal damage to the parts such as burn, marks, metallurgical phase transformations, softening of the surface and possible re-hardening, microcracks, residual tensile stress and reduced fatigue strength, which can therefore compromise the quality of the surfaces (Malkin and Guo, 2007, 2008).

A way of quantifying the grinding severity is by means of the equivalent chip thickness (h_{eq}) (Malkin and Guo, 2008), which calculation can be obtained from the (15) for surface grinding and from the (16) for cylindrical grinding (Marinescu *et al.*, 2007).

$$h_{eq} = ae\frac{v_w}{v_s} \tag{15}$$

$$h_{eq} = \frac{\pi \cdot d_w \cdot v_f}{v_s} \tag{16}$$

In which:

h_{eq}: equivalent chip thickness, µm,

ae: radial depth of cut, µm,

v_w: workspeed, m/s,

v_s: cutting speed, m/s,

d_w: external diameter of the workpiece, mm,

v_f: feed rate, mm/min.

The equivalent chip thickness represents the thickness of the material layer (chip) that is removed at a specific removal rate (Q'_w) and as a function of the cutting speed (v_s). The specific removal rate represents the rate of work material removal per unit width of contact and it is obtained from for surface grinding and from.

$$Q'_w = ae \cdot v_w \tag{17}$$

$$Q'_w = \pi \cdot d_w \cdot v_f \tag{18}$$

In general, the higher the chip thickness, the worse the surface finish. However, temperatures in the grinding zone are dependent not only on the specific energy, but also on the heat flux, partition ratio, geometry, kinematics, grinding wheel contact time, etc. For example, it is possible to observe larger temperatures even at low values of Q'_w. That is the reason why thermal damages, such as burn, are hard to predict and generalize and research works about those subjects tend to restrict their applicability for a well-defined set of equipment and assemblies (Drazumeric, Badger and Krajnik, 2014).

Surface finish of machined workpieces determine the quality of the material because it affects fatigue strength, corrosion resistance, and tribological properties. Therefore, it is of utmost importance that roughness is within strict parameters for some applications. High values of surface roughness decrease the fatigue life (Asiltürk and Çunkaş, 2011). To qualify surface quality, three main roughness parameters can be described (Marinescu *et al.*, 2007):

- R_a: arithmetic average roughness;
- R_t: the maximum difference between peak height and valley depth;

- R_z: arithmetic average between the highest peak and lowest valley in each sampling length.

Several papers presented the impact that grinding parameters cause on the surface quality, some as cited next. Sarikaya and Gullu (2014) studied the effect of cutting speed, feed rate, cooling, and radial depth of cut on the average roughness and concluded that the feed rate and the cooling condition have the highest influence on roughness. Molaie, Akbari and Movahhedy (2016) compared the influence of different types of lubrication and concluded that MQL using nanofluid combined with horizontal ultrasonic vibration reduced forces by around 60%. Sinha *et al.* (2016) stated that average roughness values are higher for burnt surfaces than for un-burnt surfaces. Thanedar *et al.* (2017) affirm that the workspeed directly influences grinding burn because it controls the dissipation of heat on the surface and they showed that the higher the wheel speed, the lower the average roughness.

In addition to surface roughness analyses, evaluation of microhardness distributions on and below the machined surface is also a manner to detect thermal damage and in general there is a close relationship between visible burn (oxidation that lead to alteration in surface color) and metallurgical transformation. Batista da Silva *et al.* (2018) reported that the occurrence of grinding burn and re-hardening on the ground surfaces of mold and die steel (similar to that used in the present study) were found in those samples that presented the highest microhardness values.

3 MATERIALS AND EXPERIMENTAL METHODS

The present work is divided in two sets of experiments, which have been performed independently and aims at different observations of the parameters. In the first set, EMI has been studied on surface grinding, and in the second set, EMI has been studied on cylindrical plunge grinding. Materials and methods are presented separately in the sections 4.1 and 4.2 for the two sets, respectively.

3.1 Surface grinding

Ten workpieces of ABNT N2711 steel from Villares Metals (‘Villares Metals. Plastic mold steel - N2711M grade’, 2017) with dimensions of 60 mm x 12 mm x 15 mm were used in the grinding tests. The hardness of such samples was (40 ± 2) HRc and the composition of the material is shown in Table 1. That type of steel is usually employed to manufacture molds in plastic injection process and is highly susceptible to thermal damages.

Table 1 – Chemical composition (% in weight) of the ABNT N2711 steel grade

C	Mn	Cr	Mo	Ni	V
0.56	0.70	0.70	0.30	1.56	0.075

Source: Villares Metals. Plastic mold steel - N2711M grade (2017)

The surfaces of the workpieces were cleaned up by using 50% isopropyl alcohol and piezoelectric diaphragms (PZTs) were glued on their surfaces by using cyanoacrylate glue, as shown in Figure 2. The PZTs are manufactured by Murata, 7BB-12-9 model, and they consist of a metal (brass) disc with diameter of (12.0±0.2) mm and thickness of (0.10±0.05) mm, in which a PZT ceramic disc (active element) with diameter of (9.0±0.6) mm and thickness of (0.12±0.10) mm is sustained. The discs form the electrodes of the transducer and are isolated between them. A wire was welded onto each electrode and the diaphragms were covered with Vaseline and silicone rubber to exclude the effects of humidity and increase mechanical resistance.

Figure 2 – Workpieces and piezoelectric diaphragms that were prepared for the tests

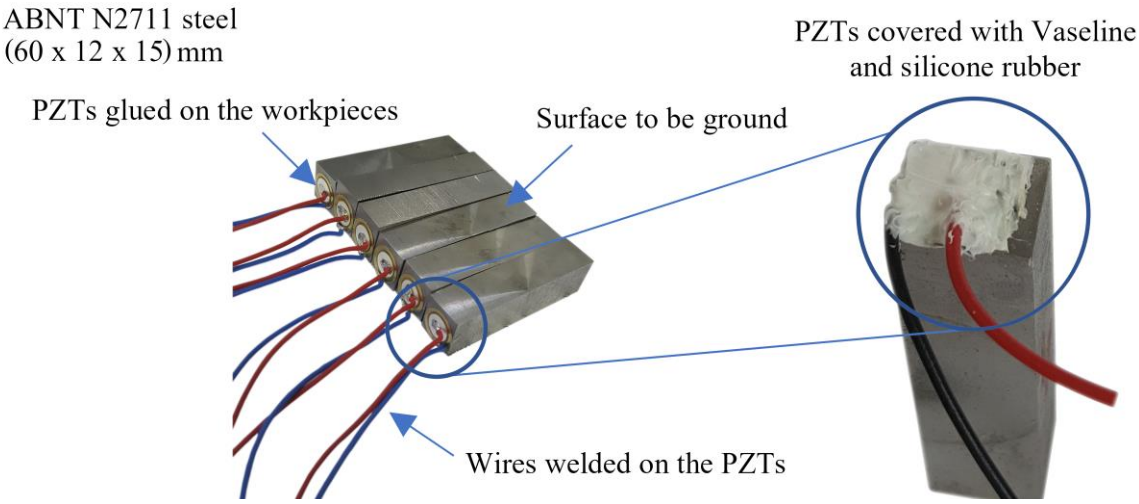

Source: Prepared by the author.

The wires from the PZTs were connected to the monitoring system which contains a data acquisition (DAQ) board, model USB-6221, from National Instruments, which was connected to a personal computer with the LabVIEW software. EMI measurements were performed in Sao Paulo State University, Bauru campus, before and after the grinding tests in a controlled environment. Each workpiece was placed on a foam inside a polystyrene box to avoid external vibrations and to keep the temperature inside the box constant during the measurement. For this purpose, the box was insulated during the measurements. Temperature inside the room was kept constant at 24.0 °C by using air-conditioned equipment and temperature inside the box was monitored by using a thermometer, MT-455 model, from Minipa and a type K thermocouple. The test bench for the EMI measurements that was used in the present work is illustrated in Figure 3. The current limiting resistor is R_S = 2.2±0.05 kΩ. The DAQ board generates a chirp signal through its analog output pin with frequencies varying from 0 to 125 kHz and amplitude of 1 V. At the same time, the analog input pin of the board collects the response signal at a sampling rate of 250 kS/s, which satisfies the Nyquist frequency criterion, and the impedance signatures are calculated by the software. The software collected five measurements in the time-domain and the average signal was used to calculate the impedance signature (frequency domain). The software interface and the algorithm that was used in the present work to collect EMI signals was developed by Baptista and is discussed in Budoya and Baptista (2018).

Figure 3 – Schematic for the EMI tests

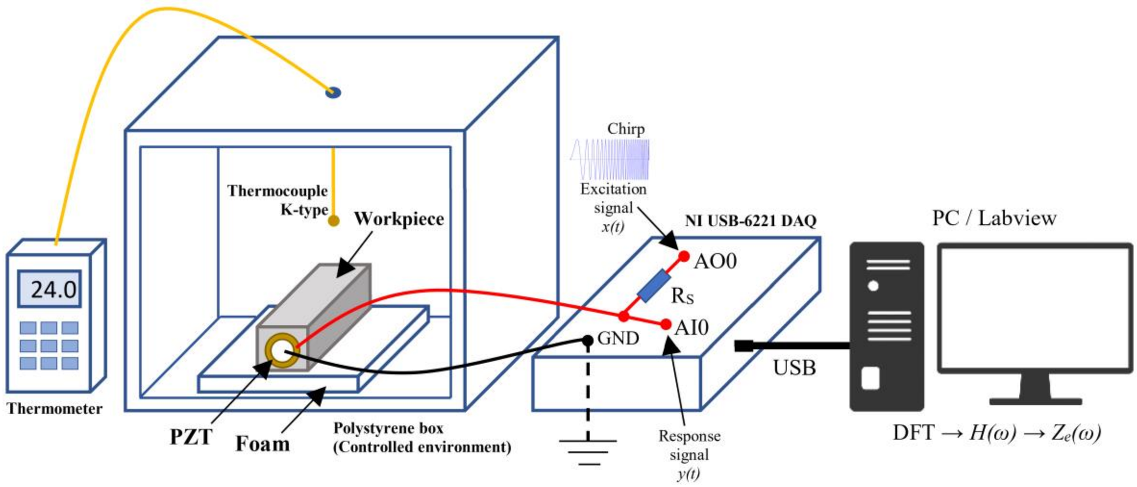

Source: Prepared by the author.

This process was performed prior to grinding (baseline signature) and after grinding, so that changes on the signature amplitude and shape can be observed for each sample. The modifications between the signatures were analyzed by using the RMSD and CCDM indices damages. Several frequency bands were studied by considering ranges of 5 kHz and 10 kHz of the real part and imaginary part of the impedance. Despite the analysis of the real part is mentioned as the favorite by the literature (Park *et al.*, 2003; Baptista *et al.*, 2013; da Silveira, Campeiro and Baptista, 2017), the imaginary part was investigated in the present study because temperature was maintained constant in the controlled environment and the objective here is to observe correlations between the phenomena.

Surface grinding, average roughness, and power tests were performed at the Federal University of Uberlandia. Surface grinding procedures are presented in Figure 4 and were performed in a peripheral surface grinding machine, P36 model, from Mello manufacturer, equipped with a conventional aluminum oxide grinding wheel, AA60K6V model, manufactured by Norton. The wheel speed (v_S) of 36 m/s was kept constant for all the tests. A semi synthetic

Vasco 7000 (vegetable based) oil, from Blaser Swisslube, was used for the tests in a proportion of 1:19 (oil to water) at a flow rate of 8.7 l/min. The wheel was dressed before each test by using a single-point dresser with overlap ratio (U_d) of 5 and dressing depth (*ad*) of 20 µm.

Figure 4 – Test bench for the surface grinding process

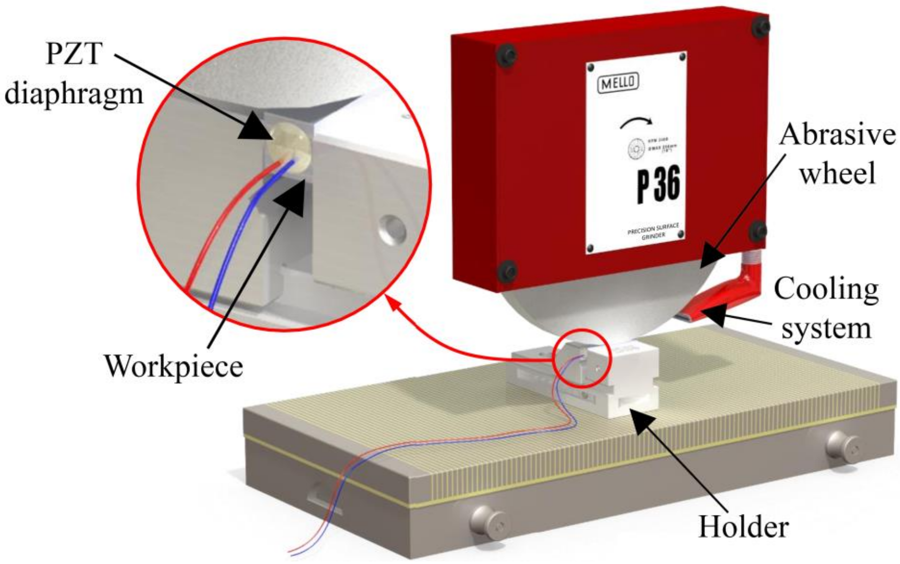

Source: Prepared by the author.

Ten samples were ground with different machining parameters to obtain 5 conditions, to ensure repeatability, with a wide range of equivalent chip thickness (h_{eq}). The experimental parameters for each test are presented in Table 2.

Table 2 – Test parameters for the surface grinding process

Condition	v_w **(m/min)**	***ae*** **(µm)**	h_{eq} **(µm)**
C1	2.4	15	0.017
C2		25	0.028
C3	5	15	0.035
C4		25	0.058
C5		50	0.116

Source: Prepared by the author.

Simultaneously with the grinding process, power signals were collected by using the Hall effect sensor HAS 50-600S model for the electric current signal and LV-20p model for the voltage signal. The DAQ NI 6001 model from National Instruments was used to collect the signals at the sampling rate of 20 kS/s. The mean value of the power signal was calculated for each sample.

After the grinding process, the microhardness on every machined surface was measured by using the tester HM-211 model, from Mitutoyo, as shown in Figure 5. Microhardness values were obtained with a load of 1.981 N ($HV_{0.2}$) for 10 seconds. Nine equidistant microhardness measurements were taken for each sample on the ground surface and the mean value for each one was computed.

Figure 5 – Microhardness measurement for the ABNT N2711 steel

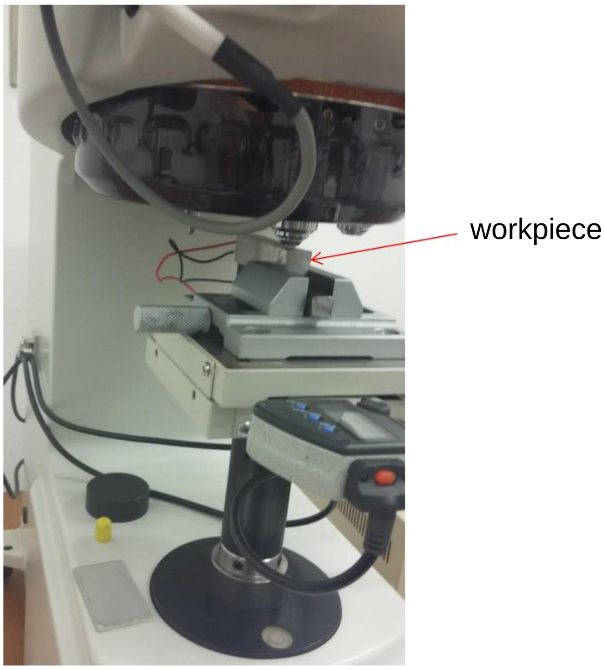

Source: Prepared by the author.

Moreover, the surface roughness (R_a parameter) was also measured after the grinding process by using the SJ201P from Mitutoyo manufacturer at a room temperature of 20.0 ± 1.0 °C, with cut-off 0.8 mm and length 5.0 mm, as shown in Figure 6. Three equidistant roughness values were measured from each sample and the mean value for each of them was calculated. These measurements were collected perpendicularly to the marks left by the abrasive grits.

Figure 6 – Surface roughness measurement for the ABNT N2711 steel

Source: Prepared by the author.

To compare parameters of different scales, all the parameters have been linearly normalized by the min-max feature scaling, which is a statistical adjustment to bring the values into the range [0, 1]. This adjustment was calculated by using the (19).

$$x' = \frac{x - x_{min}}{x_{max} - x_{min}} \qquad (19)$$

In which:

x': value adjusted into the interval [0, 1],

x: value to be adjusted,

x_{min}: minimum value of the series,

x_{max}: maximum value of the series.

3.2 Cylindrical grinding

All grinding cylindrical tests have been conducted in Kansas State University, Polytechnic campus, as well as electromechanical impedance measurements.

Eight workpieces (called lobes) of AISI – SAE 4340 alloy steel (AMS 6415) with dimensions of 56 mm x 28 mm (diameter x width) were properly prepared for the cylindrical grinding tests. This material is usually employed to build automotive systems, commercial and military aircraft parts, forged steel crankshafts, forged hydraulic, and several other machine applications. According to the manufacturer TW Metals, the Brinell hardness of the samples was (207 ± 5) HB and the composition of the material is presented in Table 3.

Table 3 – Chemical composition (% in weight) of the AISI SAE 4340 steel grade

C	Mn	P	S	Si	Cr	Ni	Mo	Cu	Al	Pb	Sn
0.42	0.76	0.006	0.005	0.26	0.86	1.79	0.27	0.24	0.028	0.001	0.01

Source: 4340 ALLOY BAR (no date)

A hole of 15 mm diameter was drilled throughout the transversal sections of each lobe and a keyway was built. A shaft was fitted into the lobe to facilitate the grinding process. The dimensions of the shaft were 15.9 mm x 150.0 mm (diameter x length). Two round shallow holes with dimensions of 15.9 mm x 5.0 mm (diameter x depth) was drilled on each surface of the lobes to allow attachment of the PZT diaphragms. All the lobes were subjected to quenching followed by tempering by using a Thermolyne type 10500 furnace. The final hardness was (46.5 ± 0.9) HRc, which was measured by a Rockwell hardness tester from Wilson – Mechanical Instrument Division, shown in Figure 7, by using a 120° diamond spheroconical Brale indenter and a load of 150 kgf.

Figure 7 – Hardness measurements setup (a) Rockwell hardness tester, (b) details of the indenter

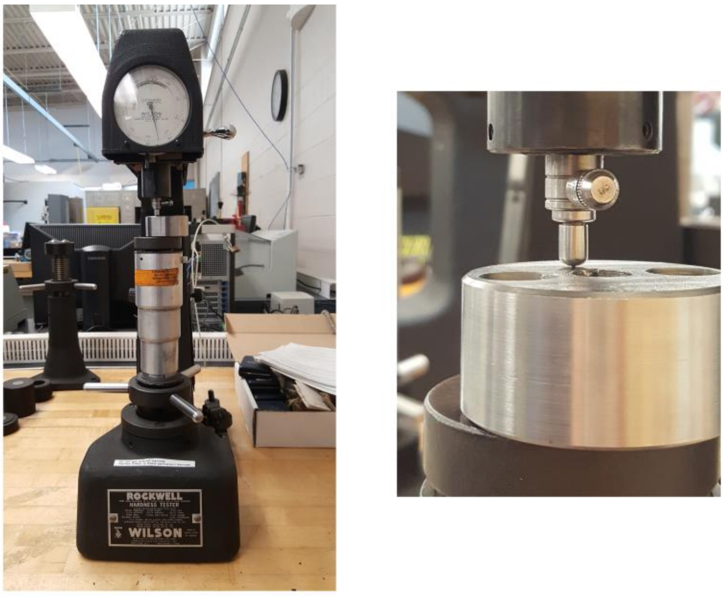

(a) (b)

Source: Prepared by the author.

Details of the heat treatment employed in this work are:

- Quenching: austenitizing at 843 °C for 60 minutes; quenching in oil.
- Tempering: heated up at 246 °C for 2 hours; cooling in air.

The workpieces during the heat treatment are shown in Figure 8.

Figure 8 – Heat treatment (a) furnace during austenitizing, (b) workpiece after heat treatment

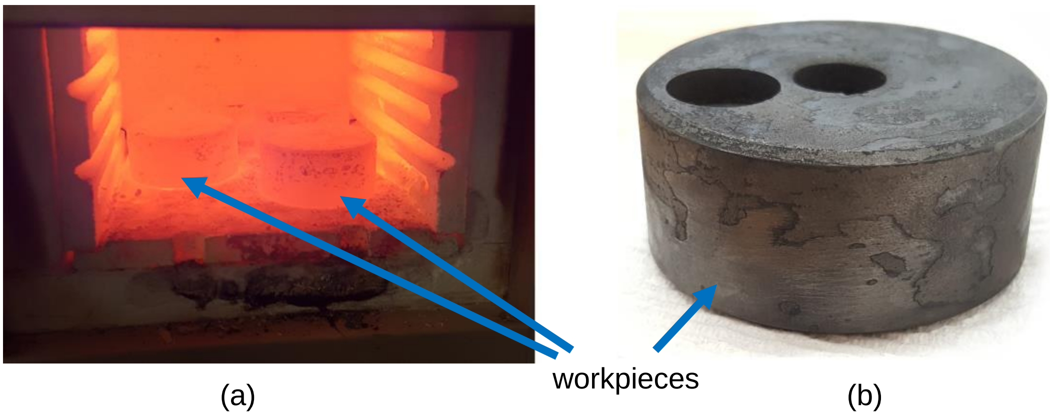

(a) (b)

Source: Prepared by the author.

Low-cost PZT diaphragms similar to those described in the previous section, 7BB-12-9 model from Murata Manufacturing, were used to monitor the workpieces. Electrical wires were welded in each pole of the transducers and they were glued at the bottom of the holes using cyanoacrylate glue. Two transducers were used for each workpiece to generate redundancy. The holes where the PZTs were placed were filled with Ultra Blue silicone gasket maker, from Permatex, to avoid influence of the coolant and humidity and to increase mechanical resistance of the weld. These steps to prepare the workpieces are shown in Figure 9.

Figure 9 – Steps to prepare the workpieces for the cylindrical grinding experiments (a) workpieces with the holes and the shaft, (b) PZT diaphragm, (c) PZT glued in the hole, (d) hole covered with silicone

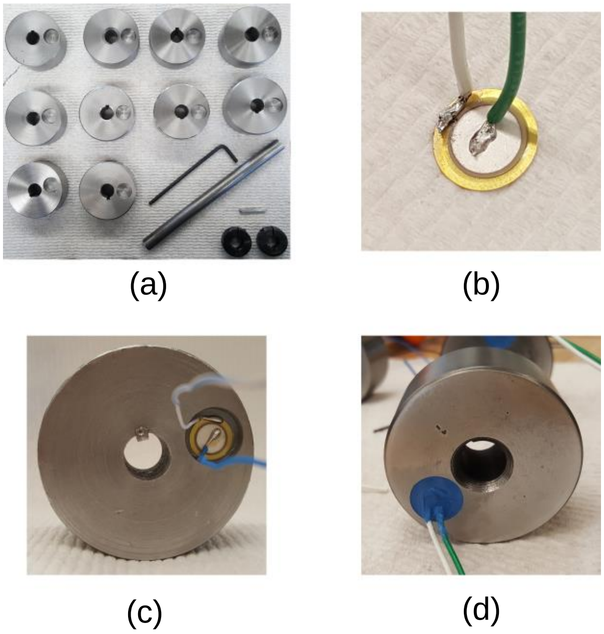

Source: Prepared by the author.

The grinding tests were conducted at the Kansas State University Polytechnic campus, by using a CNC Camshaft Grinder, 8655 model from Sherline, which is usually used to produce lobes for small camshafts employed in power plants of miniature unmanned aircraft systems. This machine was equipped with an AC motor which rotates up to 10,000 rpm and a power of 0.5 H.P. A conventional abrasive grinding wheel of aluminum oxide (Al_2O_3), 06293062 model, from Tru-Maxx, with designation 28A60K6V31 and dimensions of 152.4 mm x 6.35 mm x 31.75 mm (external diameter x thickness x hole diameter) was attached to the motor shaft. This grinding wheel has vitrified bond type, 6-structure, 60 grit surface and K hardness. All the grinding tests were performed with the nonchlorinated semi-synthetic coolant, MicroSol 585XT, with machine-friendly characteristics, from Master Fluid Solutions, in the concentration of coolant to water of 8% directed to the grinding zone by an adjustable flexible nozzle at the flow rate of 6.5 l/min. The setup used for the grinding tests is shown in Figure 10.

Figure 10 – Setup for the cylindrical grinding tests

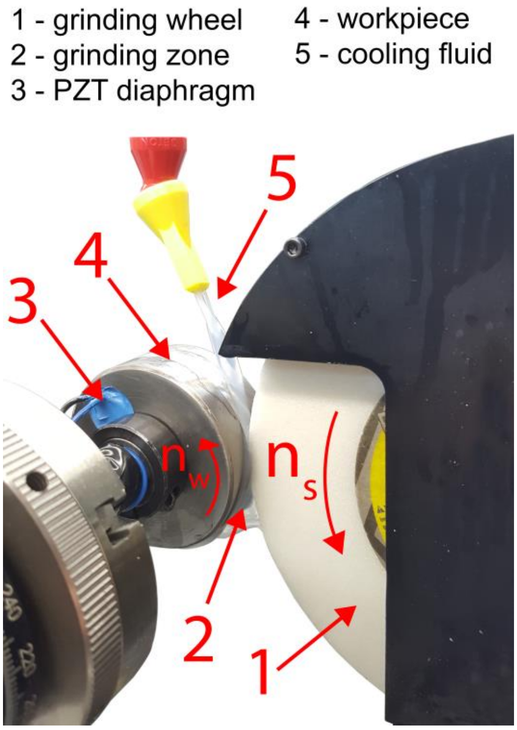

Source: Prepared by the author.

The design of experiments (DOE) was planned to obtain different surface conditions for each workpiece, by varying the radial feed rate (v_f) and the workspeed (v_w), as shown in Table 4. The wheel speed (v_s) was kept constant at 30 m/s, as well as the radial depth of cut (*ae*) at 25 µm. High values (> 100) for the ratio of grinding wheel/workspeed (q_s) were adopted to define the finishing operation and to obtain low values of surface roughness. Hence, a wide range of equivalent chip thickness (h_{eq}) was covered to obtain different grinding severities.

Prior to the grinding tests, every workpiece required preparation passes until the grinding wheel touches evenly the whole circumference of the lobe. The parameters for preparation are shown in Table 5. The initial preparation was necessary to reduce variations of roundness and surface irregularities.

Table 4 – Experimental parameters for the cylindrical grinding tests

Workpiece n°	**v_f (mm/min)**	**v_w (m/s)**	**v_s (m/s)**	**ae (μm)**	**q_s**	**h_{eq} (μm)**
1	0.1	0.1	30	25	300	0.01
2	0.5					0.05
3	0.7					0.07
4	1.0					0.10
5	0.1	0.25			120	0.01
6	0.5					0.05
7	0.7					0.07
8	1.0					0.10

Source: Prepared by the author.

Table 5 – Experimental parameters for the cylindrical grinding preparation

v_f (mm/min)	**v_w (m/s)**	**v_s (m/s)**	**ae (μm)**	**q_s**	**h_{eq} (μm)**
0.1	0.25	30	10	120	0.01

Source: Prepared by the author.

Since the Sherline machine is not equipped with a motor to control the dressing speed (v_d), the grinding wheel was dressed by using a multi-point diamond dresser, shown in Figure 11, after the preparation passes because this type of dresser reduces the influence of the macro-effect.

Figure 11 – Multi-point diamond dresser; (a) dresser body, (b) dresser head

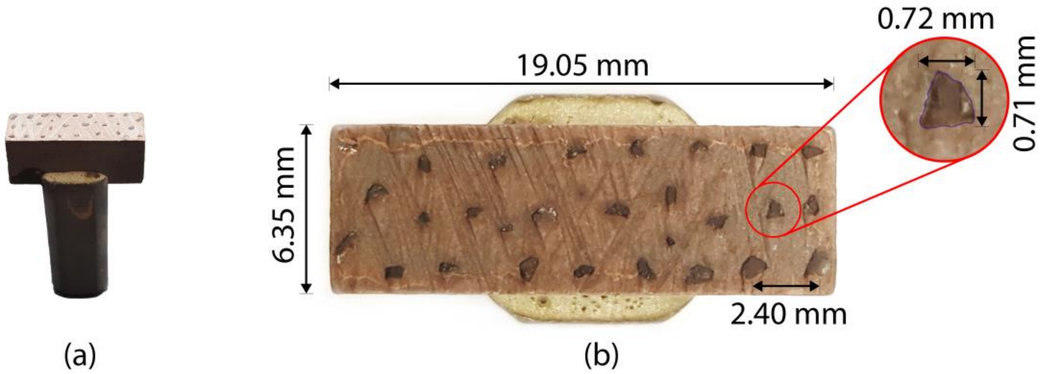

Source: Prepared by the author.

According to Malkin and Guo (2008), the thread profile on the grinding wheel, which is dependent on v_d, is relevant when single-point dresser is employed. For this reason, when multi-point dresser is used, the dressing speed does not play significant impact and a predominance of the micro-effect is observed. Therefore, the transverse movement of the dresser across the grinding wheel was performed manually by a crank handle (x_d-axis). The dimensions of the dresser are 19.05 mm x 6.35 mm (head length x head thickness). The dressing depth (a_d) was 0.05 mm, which was adjusted through a second crank handle (y_d-axis). One revolution of the second crank handle (360°) is equivalent to 1.27 mm of the dressing depth. The dressing system of the Sherline camshaft grinder is shown in Figure 12.

Figure 12 – Dressing system of the Sherline camshaft grinder

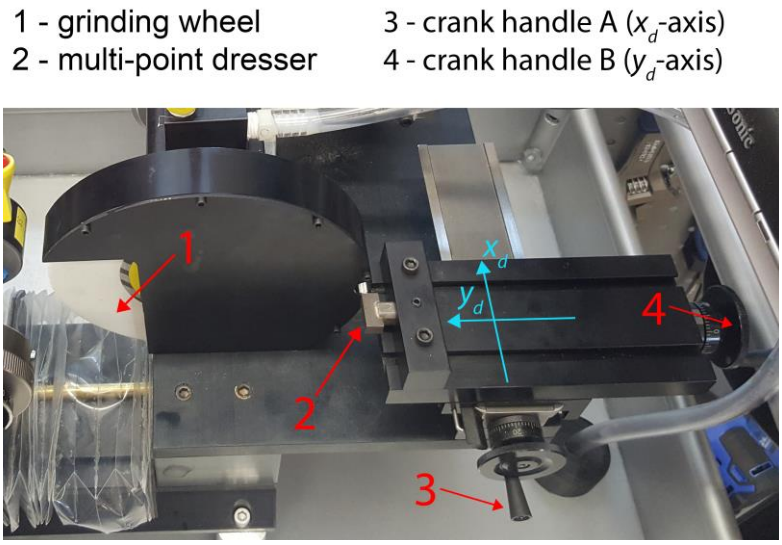

Source: Prepared by the author.

Prior and after the grinding tests, the average roughness (R_a parameter) of the round surfaces was measured by using the Mitutoyo Surftest – 402 equipment. This parameter has been chosen because it is universally adopted as an international parameter for roughness evaluation in machined surfaces. The range of the measurements was 10.0 µm and filter wavelength (cut – off) of 2.5 mm were selected. Four equidistant measurements were taken for each sample, as shown in Figure 13, and the average value and standard deviation were calculated.

Figure 13 – Roughness measurements (a) setup for measurement of R_a roughness, (b) R_a roughness measurement locations on the workpiece surface

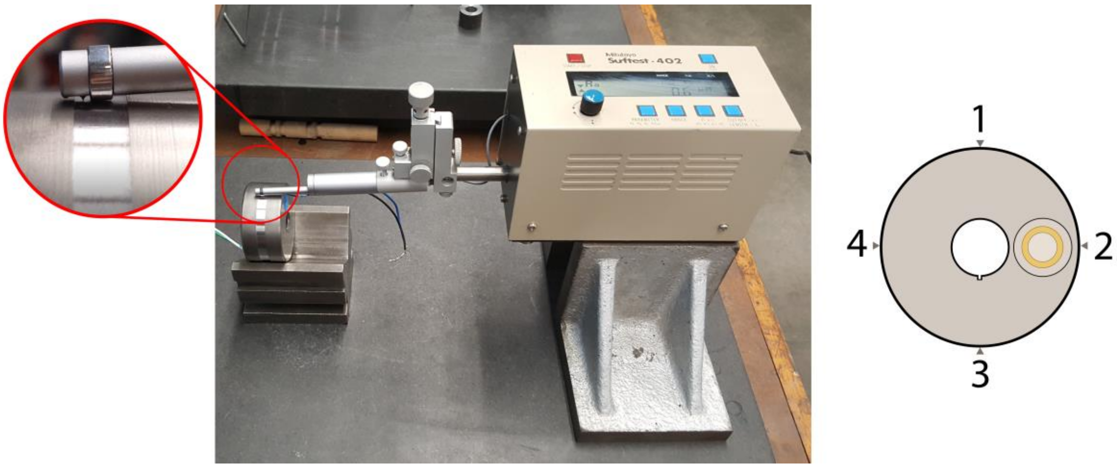

(a) (b)

Source: Prepared by the author.

The power meter, model Grindometer, manufactured by the Grinding Doc, was connected to the grinding wheel spindle motor and power signals were collected during the grinding tests using the DAQPRO-5300, from Omega. The data acquisition equipment was connected to a personal computer through a UBS port and the signals were observed and stored by the DaqLab^{TM} software. Power signals were collected at the sampling rate of 2,000 S/s (samples per second). The full scale that was adjusted at the equipment was 3 kW and the response time was 0.015 seconds. The power measurements set-up is shown in Figure 14. The average value of the power signals was calculated for each sample.

Figure 14 – The average value of the power signals calculated for each sample

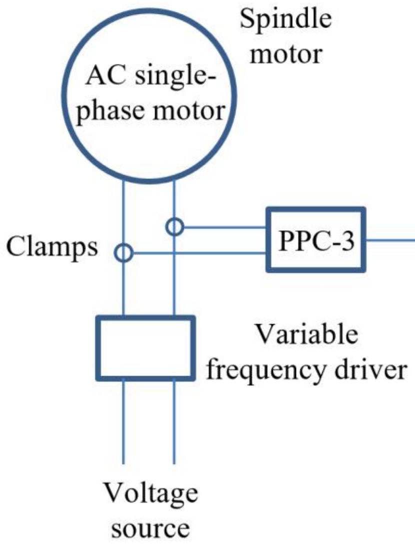

Source: Prepared by the author.

The EMI measurements were taken based on the system proposed by Baptista and Filho (2009). For each workpiece, the EMI was collected two times: prior and after the grinding process, which provided the correspondent impedance signatures, the baseline and the damaged condition, respectively. Hence, the damage level can be quantified by comparing both signatures within frequency bands by using the damage indices: RMSD and CCDM. For each workpiece, two PZT diaphragms collected impedance measurements to verify repeatability and to validate correlations between the statistical parameters.

Since the EMI technique is sensitive to external influences, such as temperature and vibrations, the EMI measurements were taken under controlled environment conditions. To this end, the workpiece was detached of the grinding wheel and the lobe was detached of the shaft. Then, the lobe (sample submitted to grinding) was placed on a foam to reduce effects of external vibrations and inside a polystyrene box to keep the temperature constant, as shown in Figure 15. The box was thermally insulated during the EMI measurements. The temperature in the room was kept constant at 20.0 ± 1.0 °C by a thermostat and the temperature inside the box was monitored by using the digital multimeter 2706A model, manufactured by B&K Precision, which was equipped with a type K thermocouple.

Figure 15 – Experimental test bench for the EMI measurements

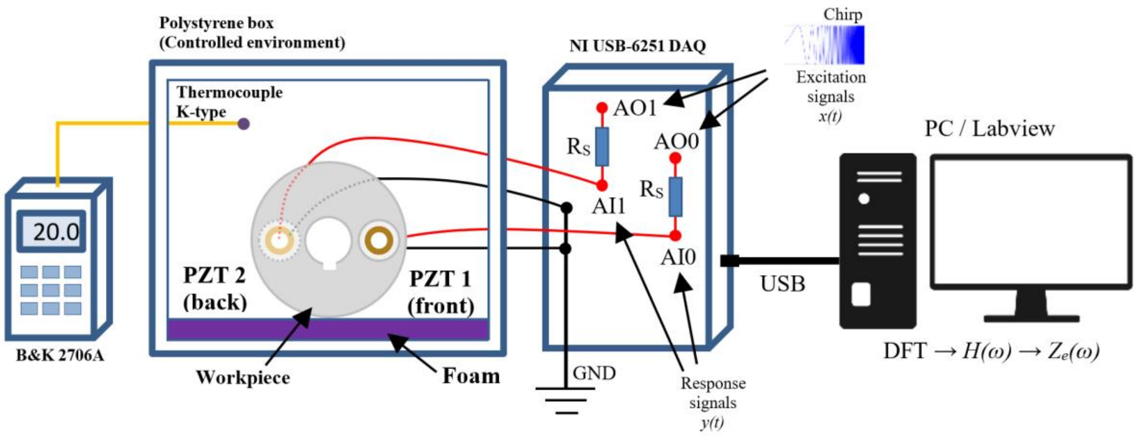

Source: Prepared by the author.

The PZT diaphragms were hooked up to the analog input (AIx) pin of the USB-6251 DAQ device from National Instruments, which was connected to a personal computer (Intel Core i7-7700HQ, 16 GB) through a USB port. Through the analog output (AOx) pin of the DAQ board, excitation signals of chirp type are generated, which have variable frequency from 0 to 200 kHz and magnitude equal to 1 V. This circuit allows to collect the response signals simultaneously with the excitation signals. The computer that was connected to the DAQ board was running the Windows operational system and was equipped with the LabVIEW package. The software that was employed to collect EMI signals was developed by Baptista and Filho (2009) on the LabVIEW interface. The sampling rate for the signals acquisition was 1 MS/s, which provided the Nyquist frequency of 500 kHz. The acquisition software internally calculated the impedance of the piezoelectric from the voltage that was collected as response to the excitation voltage. Moreover, the software collected five impedance measurements for each play and automatically calculated the average impedance signature, which was used for the analyses.

The impedance signatures are usually presented in a graph in terms of the electromechanical impedance of the structure and the frequency of the signal. Since the impedance is a complex number, it can be analyzed in terms of magnitude, real part or imaginary part. The EMI measurement obtained after the grinding operation provides a signature that differs from the healthy condition (baseline). The statistical parameters that are usually employed to quantify the variation between the healthy and damaged conditions are the RMSD and CCDM indices. In this work, the real part of the impedance was studied, and the damage indices were calculated in several frequency bands with bandwidths (bw) of 10 kHz and 5 kHz. To avoid low-frequency interferences from environment, such as the audible spectrum, the examination was conducted for frequencies above 15 kHz. The frequency bands that were used to calculate damage indices were numbered to facilitate presenting figures subsequently, as shown in Table 6 and Table 7.

The RMSD statistical parameter was employed to verify how signatures varied in amplitude, since it is related to the Euclidean distance between two signals. The CCDM statistical parameter was applied to check out shifts in frequency and shape deformations. Correlations between both transducers were studied and frequency bands that represented the surface quality through the average roughness were investigated, as well as variations of mass and power signals.

Table 6 – Labels for frequency bands from bandwidth of 10 kHz in the cylindrical grinding process

Number	Frequency band (kHz)	Number	Frequency band (kHz)
#1	[15;25]	#10	[105;115]
#2	[25;35]	#11	[115;125]
#3	[35;45]	#12	[125;135]
#4	[45;55]	#13	[135;145]
#5	[55;65]	#14	[145;155]
#6	[65;75]	#15	[155;165]
#7	[75;85]	#16	[165;175]
#8	[85;95]	#17	[175;185]
#9	[95;105]	#18	[185;195]

Source: Prepared by the author.

Table 7 – Labels for frequency bands from bandwidth of 5 kHz in the cylindrical grinding process

Number	**Frequency band (kHz)**	**Number**	**Frequency band (kHz)**
#1	[15;20]	#20	[110;115]
#2	[20;25]	#21	[115;120]
#3	[25;30]	#22	[120;125]
#4	[30;35]	#23	[125;130]
#5	[35;40]	#24	[130;135]
#6	[40;45]	#25	[135;140]
#7	[45;50]	#26	[140;145]
#8	[50;55]	#27	[145;150]
#9	[55;60]	#28	[150;155]
#10	[60;65]	#29	[155;160]
#11	[65;70]	#30	[160;165]
#12	[70;75]	#31	[165;170]
#13	[75;80]	#32	[170;175]
#14	[80;85]	#33	[175;180]
#15	[85;90]	#34	[180;185]
#16	[90;95]	#35	[185;190]
#17	[95;100]	#36	[190;195]
#18	[100;105]	#37	[195;200]
#19	[105;110]		

Source: Prepared by the author.

4 EXPERIMENTAL RESULTS AND DISCUSSION

In the present section, results and discussion have been divided in two independent parts. Section 5.1 are related to the surface grinding experiments and Section 5.2 refers to the cylindrical plunge grinding. In both, experiments are discussed by investigating the EMI measurements and the mechanical parameters.

4.1 Surface grinding

In this section, results of the surface grinding are presented. First, correlation between severity of grinding (equivalent chip thickness), instantaneous power and surface quality are discussed. Then, results of the EMI are shown as impedance signatures, in which a comparison was drawn real and imaginary parts for mild and several grinding conditions. Next, damage indices results are presented for different frequency bands. Finally, correlations have been discussed between damage indices, cutting parameters, instantaneous power, and surface quality.

4.1.1 Correlation between severity of grinding and instantaneous power and surface quality

This section presents the correlation between the severity of the grinding process and the measurements that were taken during and after grinding: instantaneous power and roughness and microhardness of the workpieces. The results of the measurements are presented in Figure 16.

Figure 16 – Correlations among the parameters observed during and after the surface grinding process

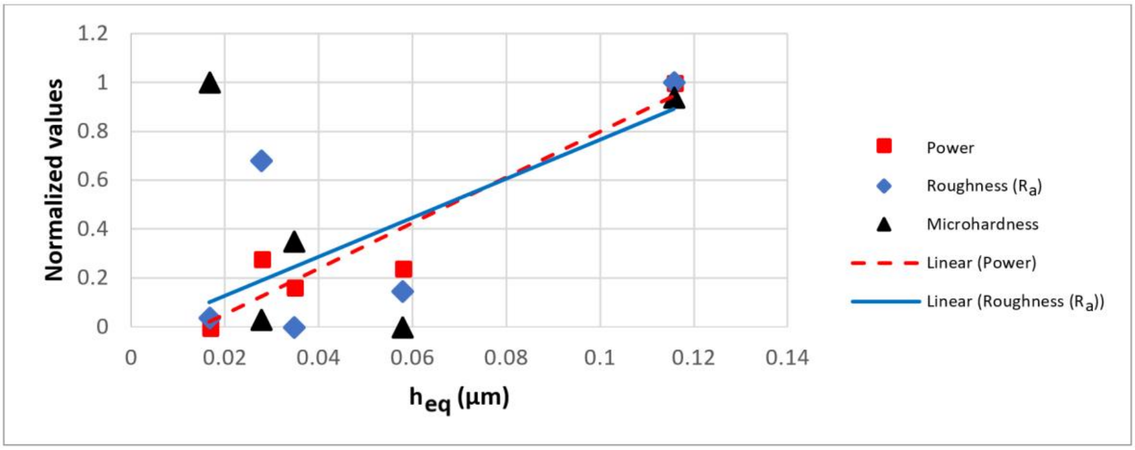

Source: Prepared by the author.

Such results were already expected in view of the parameters that were used for grinding and presented in Table 2. Since h_{eq} increases, severity of the process increases, as well as the forces between the grinding wheel and the workpiece, and more power is required from the motors. Therefore, as h_{eq} increases, the power increases as well. Moreover, the increase of the severity is followed by the increase of the roughness. Indeed, the roughness increases if v_w or *ae* increases, i.e., the surface quality of the workpiece decreases for higher values of h_{eq}. Finally, no correlation was found between h_{eq} and microhardness. In fact, one would not necessarily expect a correlation between these parameters, since it is possible to obtain good surface finish but with visible burn (condition in which changes are observed on the surface of the microstructure or below it). Changes in the microstructure of the material can be caused by thermal damages and they can modify its microhardness. For the condition h_{eq} = 0.017 µm, for example, the workspeed was the lowest one and could have led to an increase in the microhardness due to increased heat generation and chip formation though prolonged contact between the surfaces. Therefore, microhardness values depend on several factors besides severity and no correlation was found between them.

4.1.2 Impedance signatures

Frequencies below 15 kHz for the response signal were not considered in the analyzes because they contain low frequencies noises and vibrations from the external environment (Na and Baek, 2018). Examples of the real and imaginary parts of EMI signatures for two different conditions of h_{eq} are illustrated in Figure 17, representing distinct severities, which were obtained from the circuit and software developed by Baptista and Filho (2009).

At a first glance, it is easily noted that the signatures are closest to each other for the lowest value of h_{eq}. Indeed, as h_{eq} increases, which represents an increasingly severity of grinding, it is expected that the curves have larger differences between the healthy and the damaged conditions because the greatest the damage, the farther or more different in shape the signature after grinding from the baseline signature. Moreover, it is possible to note that the real part of the impedance decreases as the frequency increases. Such signature behavior shows that the resistance characteristic of the structure is higher for lower frequencies, i.e. the lower the frequency, the higher is the sensitivity for the transducer to detect damage. This behavior was also stated by Junior, D'addona, *et al.* (2018), who conducted the pencil-lead-break (PLB) test to verify the frequency spectrum of such sensor and concluded that they display more sensitivity in terms of damage detection for frequencies below 200 kHz. On the other hand, the imaginary parts of the impedances are very close to each other (before and after grinding), which denotes low sensitivity to detect damages. In fact, this is also observed in the next section by observing the damage indices. The imaginary part has negative values for lower frequencies, which represents predominance of the capacitive reactance effect due to the structure of the PZT diaphragm formed by two polarized and isolated discs causing an electric field, as also stated by Park *et al.* (2003). The imaginary part tends to zero for high frequencies (Baptista and Filho, 2009), as it is already known that the behavior of capacitors is given by $|X_C| = 1/(2\pi fC)$, i.e. as the frequency increases, the module of the capacitive reactance tends to zero.

Figure 17 – examples of EMI signatures for different conditions in the surface grinding process

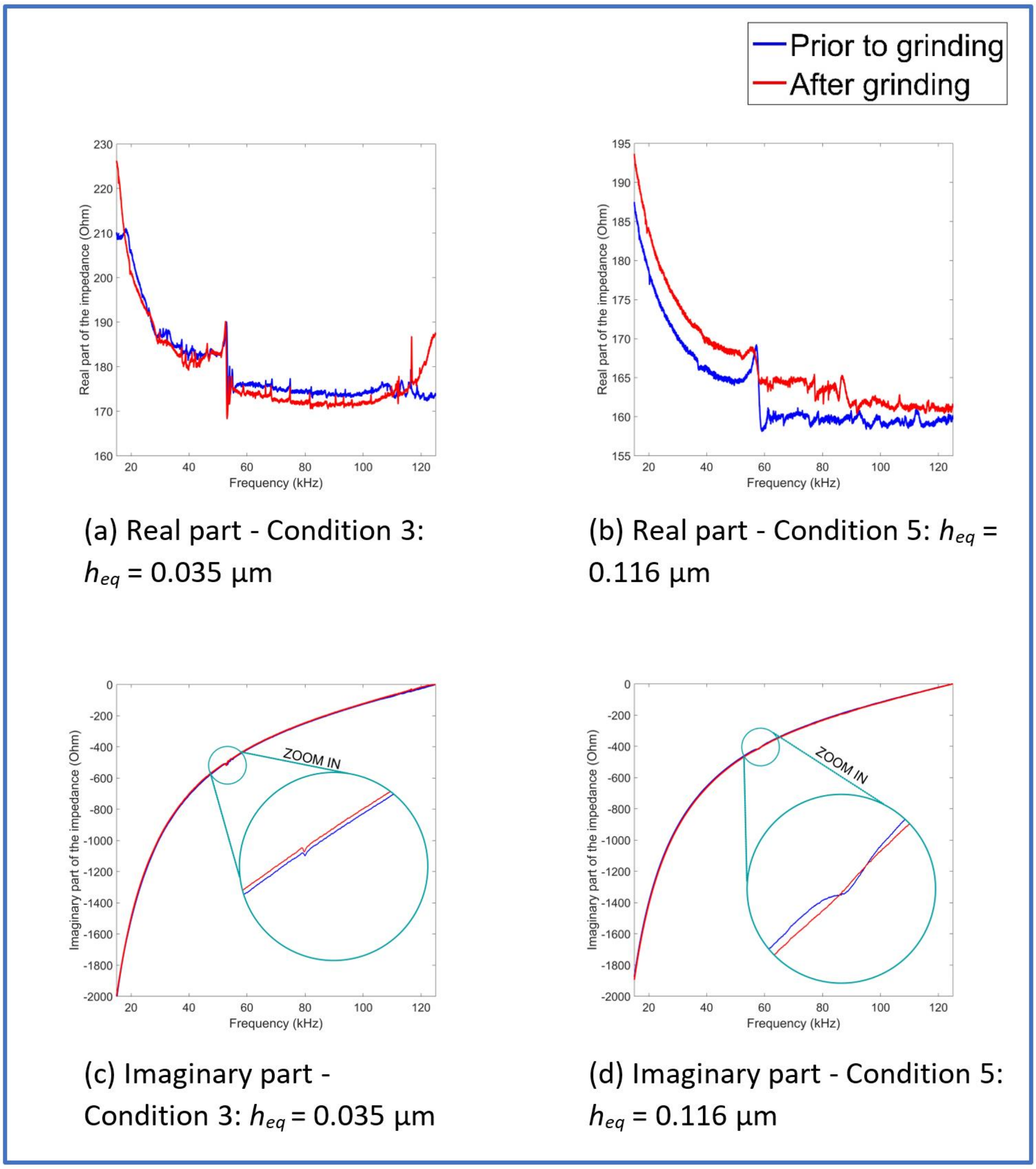

(a) Real part - Condition 3: h_{eq} = 0.035 µm

(b) Real part - Condition 5: h_{eq} = 0.116 µm

(c) Imaginary part - Condition 3: h_{eq} = 0.035 µm

(d) Imaginary part - Condition 5: h_{eq} = 0.116 µm

Source: Prepared by the author.

4.1.3 Damage Indices

The damages indices RMSD and CCDM were calculated for several frequency bands, considering windows lengths of 5 kHz and 10 kHz, from the real and imaginary parts of the EMI signatures, as shown in Figure 18. As previously mentioned, imaginary part was also analyzed because influences of temperature are reduced in controlled environment.

It is possible to note that the indices presented some high values for some high frequency bands (considering the frequency range analyzed of 15-125 kHz), which was not expected. This was also stated by Junior, D'addona, *et al.* (2018), who observed that damage indices showed more sensitive for the higher frequencies in the frequency spectrum that was studied. However, more appropriated bands were found for intermediary frequencies, in which increasing tendencies of the indices could be correlated with the increasing severity and other mechanical parameters, as discussed in the next section. For the lowest severity, high RMSD indices were found as frequency bands increase, i.e., the signatures before and after grinding moved away from each other in high frequencies. It is a surprising statement and could be related to heat generated and chip formation for this condition, as the workspeed is the lowest for this condition. Higher temperatures impact directly over the structure of the material and can cause thermal damages, e.g. changing its hardness, as will be presented in the next section. However, those frequency bands can be deeply explored in future works aiming at thermal damages in the structure of the material.

Figure 18 – Damage indices from EMI signatures for different frequency bands in the surface grinding process

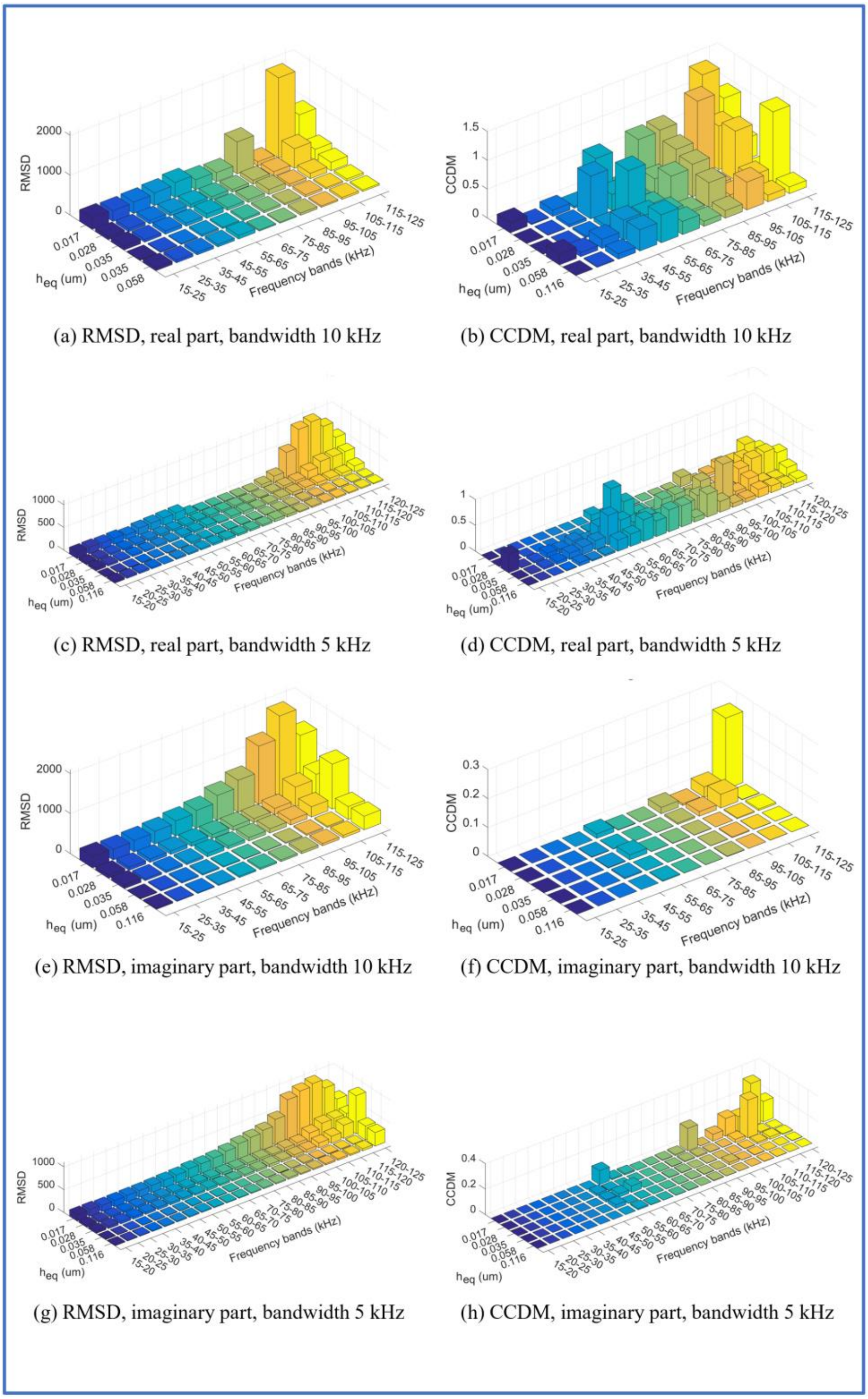

(a) RMSD, real part, bandwidth 10 kHz (b) CCDM, real part, bandwidth 10 kHz

(c) RMSD, real part, bandwidth 5 kHz (d) CCDM, real part, bandwidth 5 kHz

(e) RMSD, imaginary part, bandwidth 10 kHz (f) CCDM, imaginary part, bandwidth 10 kHz

(g) RMSD, imaginary part, bandwidth 5 kHz (h) CCDM, imaginary part, bandwidth 5 kHz

Source: Prepared by the author.

4.1.4 Correlation between EMI indices and the cutting parameters

In this section, the correlation between the damage indices of the EMI technique and the cutting parameters that were theoretically defined for the tests, h_{eq}, *ae*, and v_w is discussed. Normalized values (by using the min-max featuring scaling) of the damage indices for some frequency bands with increasing tendency for the real part of the impedance are presented in Figure 19.

Figure 19 – Correlation between h_{eq} and damage indices in the surface grinding process

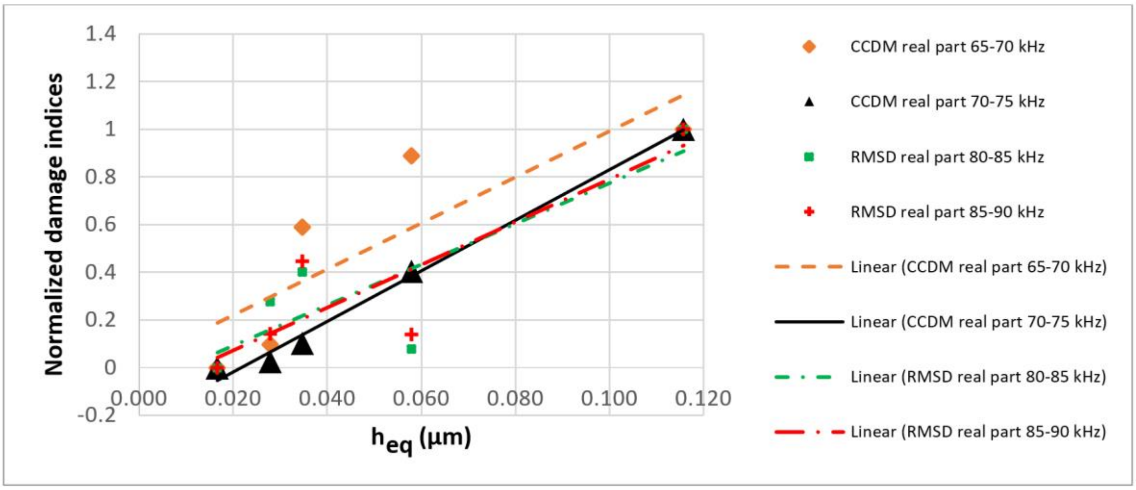

Source: Prepared by the author.

No increasing tendencies were found for the imaginary part, so none of them was presented in that figure. A decreasing tendency was found for the real part with CCDM at the band 85-95 kHz but, as previously mentioned, no justification is found to correlate increasing h_{eq} with decreasing damage indices and then it is not shown in that figure as well. Although all the situations that were presented in that figure exhibit an increasing tendency, all of them, with exception of CCDM real part 70-75 kHz, presented large deviation of some points from the average line, which does not represent accurate correlation for a monitoring system. Thus, the best correlation between h_{eq} and the damage indices was found for the real part with CCDM at the band 70-75 kHz.

The influence of the parameters *ae* and v_w separately over the damage indices for the best situation that was found, that is, CCDM real part 70-75 kHz, is presented in Figure 20.

Figure 20 – Correlation among the damage indices with *ae* and v_w for the CCDM real part 70-75 kHz in the surface grinding process

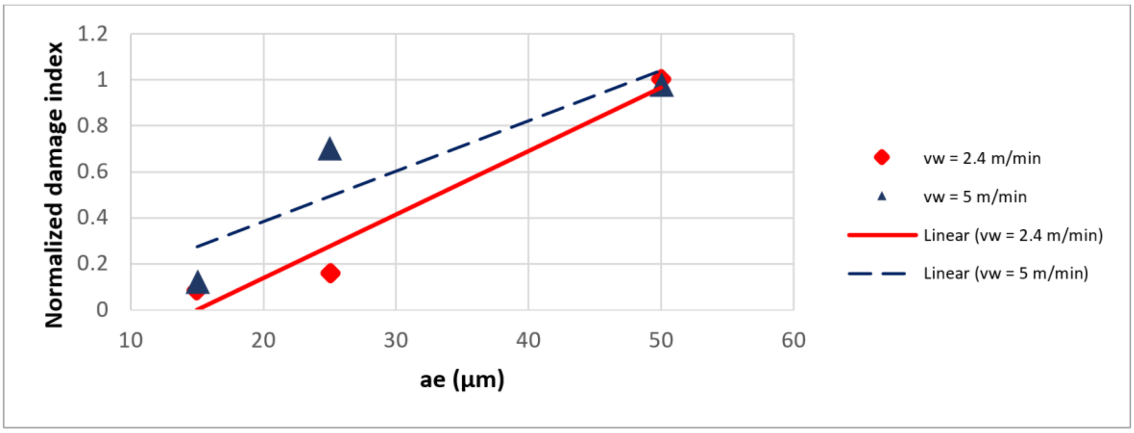

Source: Prepared by the author.

It is possible to observe that both parameters are directly proportional to the indices, i.e., the greater the *ae* values, the greater the damage indices; and the greater the v_w values, the greater the damage indices as well. Therefore, it is possible to affirm that the CCDM index calculated for the real part of the impedance at the frequency band 70-75 kHz is correlated to h_{eq}, *ae*, and v_w.

4.1.5 Correlation between EMI indices and instantaneous power and surface quality

This section discusses the correlation among the damage indices of the EMI technique, instantaneous power, and surface quality (roughness and microhardness). The best correlations found between EMI indices and power signals are shown in Figure 21.

Figure 21 – Correlation between damage indices and power signal in the surface grinding process

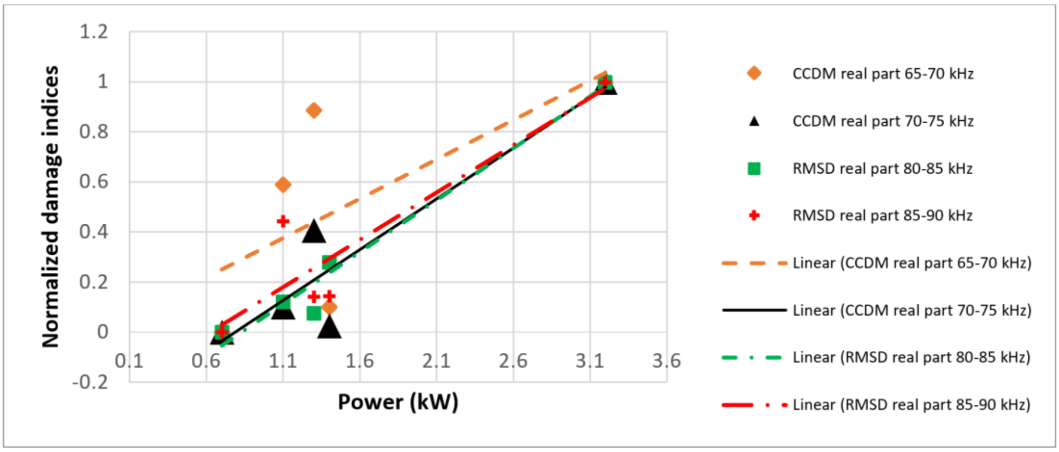

Source: Prepared by the author.

The RMSD index for the real part of the impedance in the frequency band 80-85 kHz presented the best correlation. However, new tests should be conducted to verify if the correlation between EMI indices and power signals are effective, whereas power signals are related to the severity of the process and not directly to structure health.

Correlating roughness with damage indices, the RMSD index for the real part of the impedance in the frequency band of 80-85 kHz presented the best result, as shown in Figure 22.

Figure 22 – Correlation between damage indices and roughness values in the surface grinding process

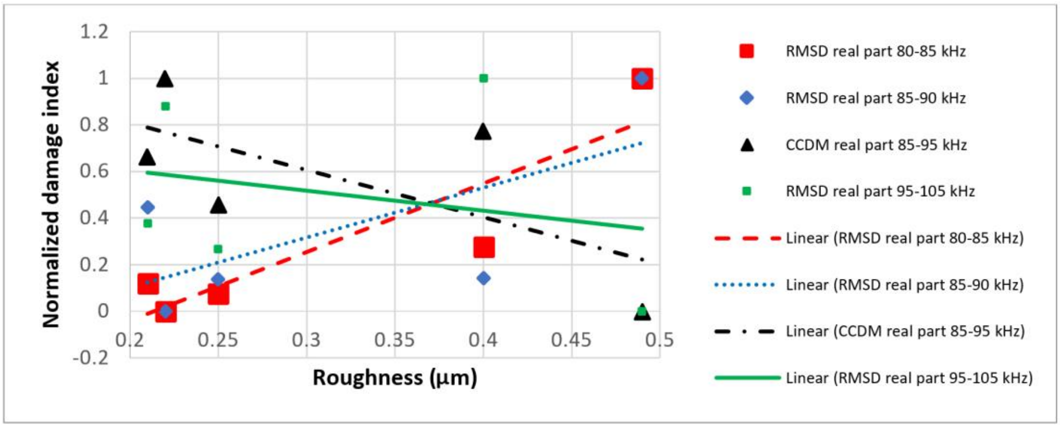

Source: Prepared by the author.

Notably, this is the same set of band and index that were found for the correlation of power and EMI indices. The correlation between roughness and EMI indices makes more sense, because roughness is directly related to the structural health. The better the quality of the surface finish, the greater the values of the indices. As the best correlation (RMSD real part 80-85 kHz) presents increasing tendency, it can be affirmed that worst surface finish causes greater changes on the EMI signature and hence larger indices. Such feature could be used to infer the workpiece quality through indirect monitoring.

Some correlations were found between microhardness and EMI, as shown in Figure 23.

Figure 23 – Correlation between damage indices and microhardness in the surface grinding process

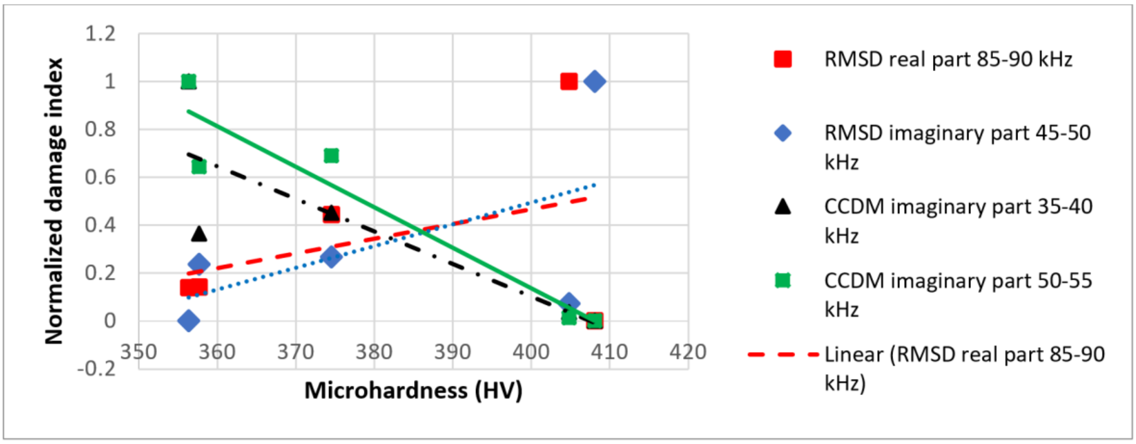

Source: Prepared by the author.

The best one was observed for the CCDM index calculated for the imaginary part of the signature in the frequency band 50-55 kHz. It is noted that the higher the microhardness value of the structure, the lower is that damage index, i.e., these parameters are inversely proportional.

4.2 Cylindrical grinding

4.2.1 Preparation of lobes for grinding

Initially, the radial depth of cut was the same for every workpiece and, consequently, the mass removed in each lobe is theoretically the same as well. The average mass removed was 2.25 ± 1.16 grams. The deviation of removed mass is due to the geometrical differences and misalignment between the workpiece samples, which were produced through turning operation and their central holes were produced through the drilling operation. Since, dimensional tolerances provided by these processes are relatively looser, centrality and concentricity deviations should be minimized prior to grinding tests. So, several grinding passes were performed until the whole workpiece perimeter had been touched by the grinding wheel, which impacted on the mass removed as well. However, the average mass removed represents 0.49% of the total mass of the workpiece, which was considered insignificant for the analysis that is proposed in this work.

4.2.2 Surface roughness

The results of the average roughness R_a recorded for all the samples after grinding operation are shown in Figure 24, which were recorded as function of the radial feed rate and two workspeed values.

Figure 24 – R_a roughness of the AISI SAE 4340 steel after cylindrical grinding with different values of feed rate and workspeed

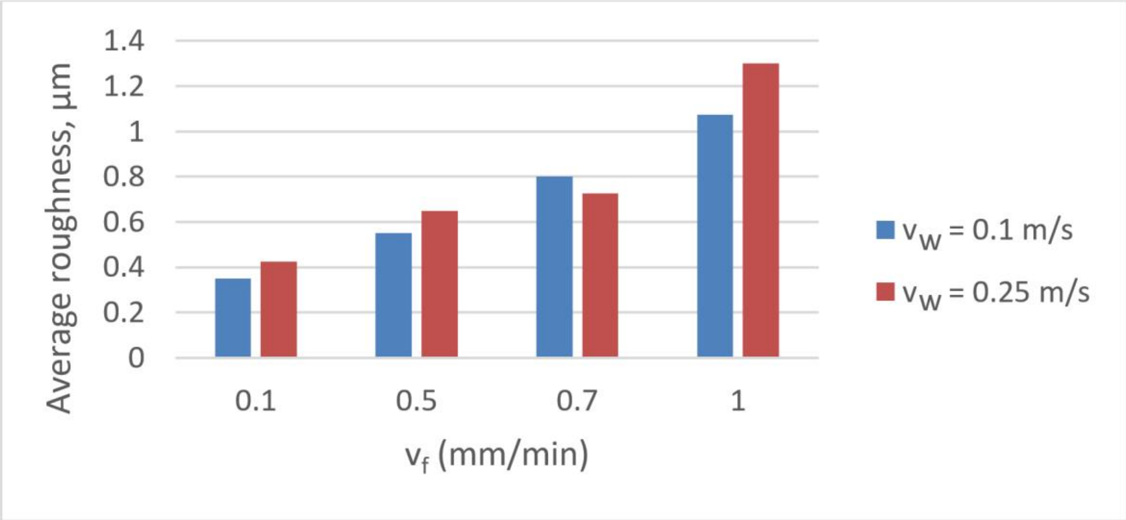

Source: Prepared by the author.

One notes that, regardless of the workspeed, the higher the feed rate, the higher the average roughness as expected. In fact, increasing feed rates cause higher equivalent chip thickness values, which is a relative measure of grinding severity (Malkin and Guo, 2008). The more severe the grinding condition, the higher it is due to the plastic deformation during cutting, which causes an increasing amount of irregularities on the workpiece surface and, hence, impairing surface roughness. However, despite the workspeed presents less influence than the feed rate on the roughness, the first also impacted on the R_a parameter, although on a smaller scale. All the R_a values are below the upper reference limit for the grinding process, which is R_a = 1.6 μm (Grote, 2019).

Two approach must be considered to analyze correlation between average roughness and workspeed:

Very low workspeed values can compromise surface quality, causing, for instance, burn, microhardness drops below the machined surface and microcracks, as well as high roughness values because of the longer contact time between workpiece and grinding wheel. This fact is mainly dependent on the thermal conductivity of the grinding wheel and material, as well as of the cooling system features.

On the other hand, higher workspeed values represent higher specific removal rate, which causes rougher chip formation, higher forces, higher equivalent chip thickness and, consequently, impaired finishing in general.

In the tests conducted by this work, R_a values increased for higher workspeed values in general. The AISI SAE 4340 steel is a good thermal conductor (thermal conductivity of 44.5 $W.m^{-1}.K^{-1}$ (AZoM, 2012)) and the flow rate of the coolant was abundant for the small contact area in the grinding zone.

4.2.3 Power signals

Grinding power monitoring provides a feasible approach to infer the parameters of the grinding process. Behavior of the power signals in terms of the feed rate and workspeed is shown in Figure 25a. Moreover, the correlation between average roughness and grinding power is shown in Figure 25b.

Figure 25 – Power results in the cylindrical grinding process

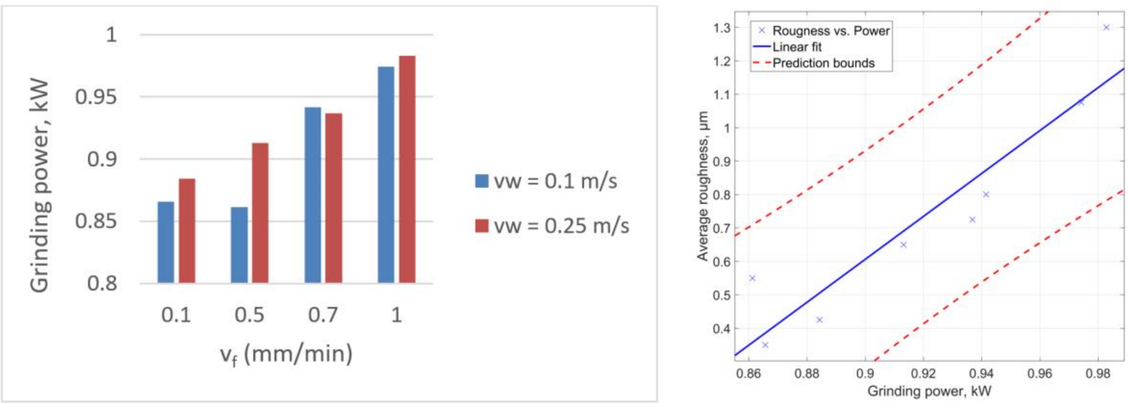

(a)
effects of the grinding parameters on the power

(b)
correlation between grinding power and average roughness

Source: Prepared by the author.

Based on the Pearson Product Moment Correlation (PPMC), the Pearson correlation coefficient between average roughness and grinding power was equal to 0.93, which indicates the linear relationship between the two sets of data (blue continuous straight line in the figure). This statistical parameter can vary from -1 to 1, in which the -1 value indicates an inversely proportional relationship, 1 indicates a directly proportional relationship, and 0 indicates that variables are not related (Fávero and Belfiore, 2017). The Root Mean Square Error (RMSE) was 0.12 µm, which shows an estimation of the standard deviation of the random component in the parameters. An RMSE value closer to 0 indicates that the fit is more useful to predict the grinding parameter based on the power signals. The dashed curves in red represent the prediction bounds for the fitted function at the level of certainty of 95%, that is, a 5% chance of being incorrect about predicting a new observation is assumed. For this prediction system, the linear model is given by R_a = 6.422P-5.173, where R_a is the average roughness, in µm, and P is the grinding power, in kW.

In fact, grinding power showed to be proportional to grinding severity. In general, high feed rate values caused high grinding power values because as feed rate increases, the specific removal rate and, equivalent chip thickness also increased, and, consequently, resulting in grinding severity. These results show that it is possible to infer the average roughness, which is one of the main parameters to quantify the surface quality, by using power signals.

4.2.4 Electromechanical impedance measurements

The real part of the electromechanical impedance signatures for two different cutting conditions are shown in Figure 26. According to the literature, the real parts have shown the best potential to be employed in monitoring systems because it is less susceptible to external influences, such as temperature (Park *et al.*, 2003; Baptista, Filho and Inman, 2010, 2012; Silva De Freitas and Guimarães Baptista, 2016). In the first subfigure, a mild cutting condition is shown and, in the second one, a severe condition. Since two PZT diaphragms were attached on each workpiece and each sensor collected signals prior to grinding and after grinding, each graph has four curves. The blue curves are the signals collected from the sensor that was attached on the front side of the workpiece and the red curves, from the sensor attached on the back side. Moreover, the dashed lines come from the signals collected prior to grinding, which represent the baseline (healthy condition), while the continuous curves represent signals collected after grinding (damaged condition).

Figure 26 – EMI signatures for different cutting conditions in the cylindrical grinding process

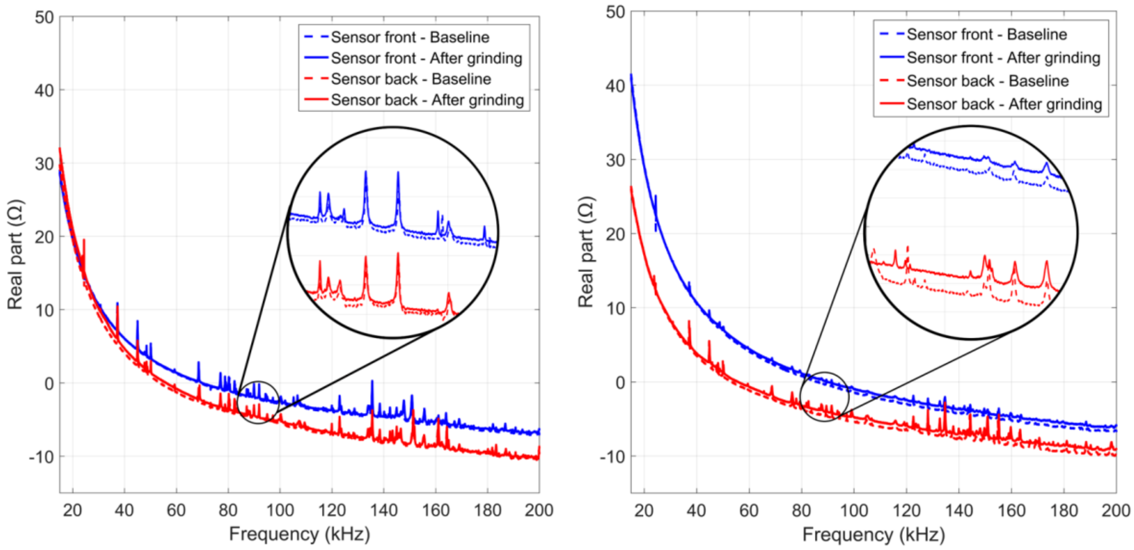

(a) mild condition – h_{eq} = 0.01 µm

(b) severe condition – h_{eq} = 0.10 µm

Source: Prepared by the author.

It is possible to note variations between signals after grinding when compared to their respective baseline. In fact, the electromechanical impedance signatures vary when structural changes are done, which is verified by amplitude variations and frequency shifts. By comparing Figure 26(a) and Figure 26(b), it was observed that the most severe condition provided greater changes between the baseline and after grinding signatures. This is noted by the highest distance between them and peak shifts when most severe cutting conditions are used for grinding.

It is also important to mention that, despite there are two PZT diaphragms attached to the workpiece, their curves are different because they are dependent on some features, such as adherence interface of the diaphragm to the structure, wires and cables, distances from the diaphragms to the material particles and damage etc. For example, Vieira Filho, Baptista and Inman (2011) observed that by varying the distance between the damage and the PZT diaphragm, the stiffness of the specimen changes and, consequently, EMI signatures vary as well. Furthermore, da Silveira, Campeiro and Baptista (2017) stated that different mounting methods of the diaphragm on the structure provides variations of the EMI signatures. Therefore, in the present work, it was already expected that PZT 1 and PZT 2 provided slightly different results, which can be used to verify repeatability and study the behavior of damage indices for the same structure, as discussed in the next section.

4.2.5 Damage indices

Alterations of the signatures (comparison between healthy condition and damaged condition) were quantified by the RMSD and CCDM indices, as presented in Figure 27 and Figure 28, respectively. Great distances between the baseline and after grinding signatures caused higher RMSD values, as well as great differences of shape of frequency shifts caused higher CCDM values. It is important to note that, in Figure 27, indices were calculated for bandwidths of 10 kHz, resulting in frequency bands numbered according to Table 6. Similarly, indices calculated for bandwidths of 5 kHz, which represents a better resolution, are shown in Figure 28 and the frequency bands were numbered according to Table 7.

It is possible to note that the RMSD index presented values below 1×10^4 for most part of the frequency bands, noticed by the predominance of the dark blue color in Figure 27 (*a* and *b*) and Figure 28 (*a* and *b*). However, indices with higher values were observed for frequencies from 45 kHz to 90 kHz for all the workpieces. Moreover, it was noticed occurrence of the highest RMSD values when using the PZT 1 for the frequency bands #6, #7, #8, and #9 (bandwidth 10 kHz), which are represented by the warmer colors in Figure 27(a). However, for the PZT 2, the highest RMSD values were found for the bands #4, #5, and #6 (bandwidth 10 kHz), as seen in Figure 27(b). Equivalent phenomenon is observed for the graphs that present RMSD index for the bandwidth 5 kHz: for the PZT 1 (Figure 28 (a)), the highest values are seen in the frequency bands from #11 to

#16, and for the PZT 2 (Figure 28 (b)), from #8 to #11. The cause of the frequency shift phenomenon of the RMSD index for all the workpieces is still unknown and will be exclusively studied in future works.

Figure 27 – Damage indices from EMI for bandwidth of 10 kHz in the cylindrical grinding process

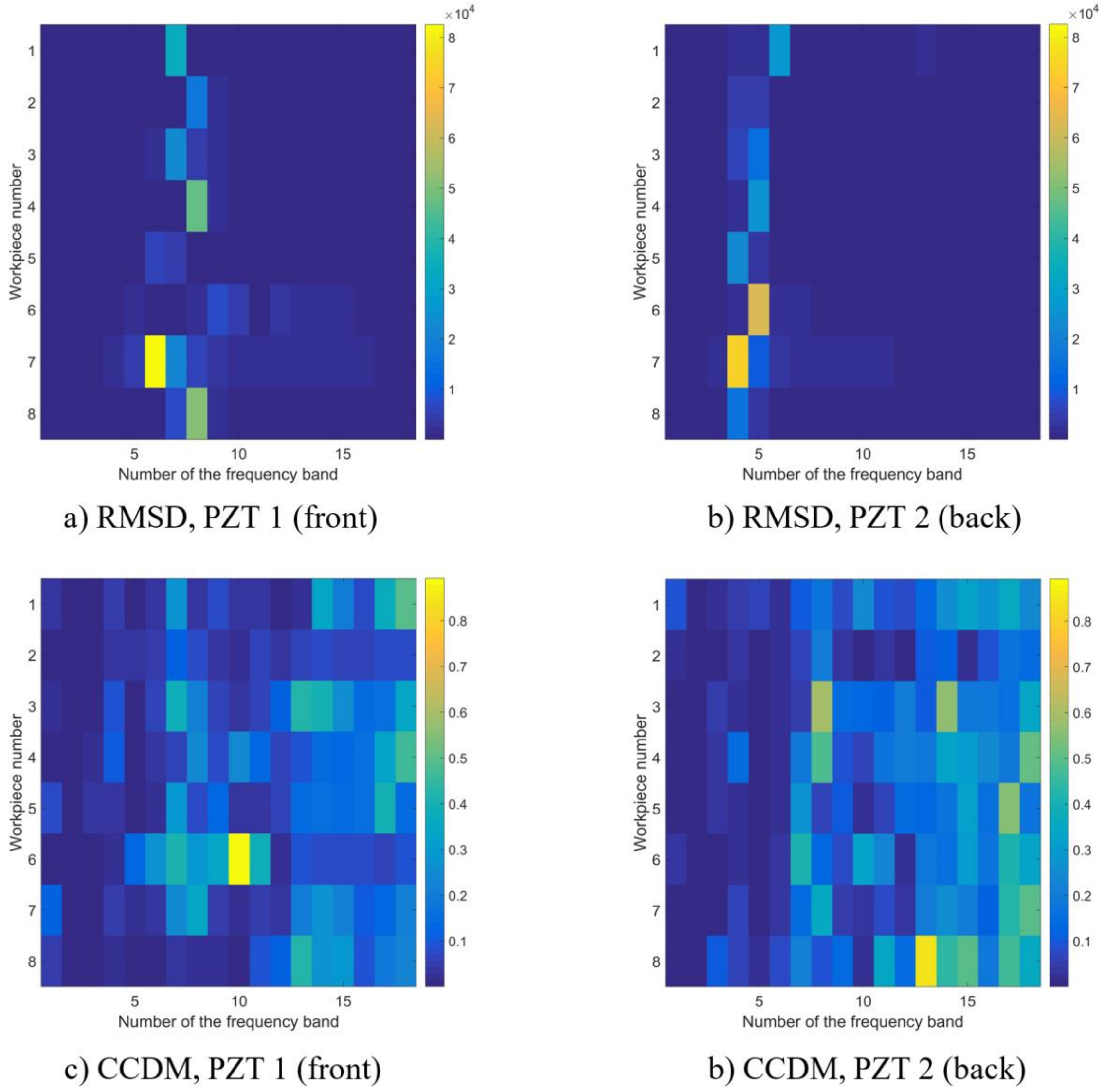

Source: Prepared by the author.

For the CCDM index shown in Figure 27 (*c* and *d*) and Figure 28 (*c* and *d*), no pattern was observed between the values. Patterns are not easily recognized because values seemed to vary randomly and they need to be analyzed through the appropriate correlation statistical parameters, as presented in the next section.

Figure 28 – Damage indices from EMI for bandwidth of 5 kHz in the cylindrical grinding process

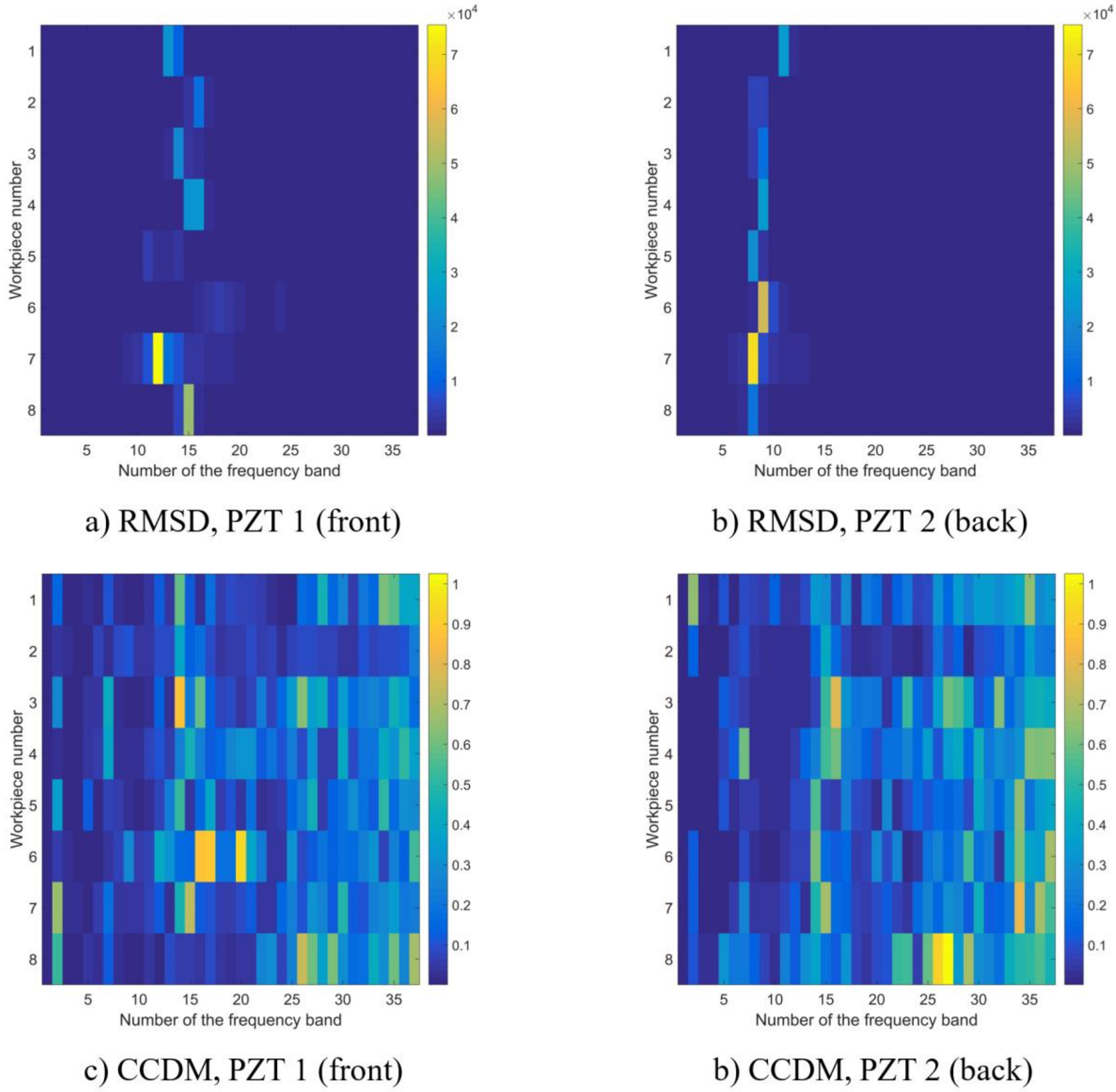

a) RMSD, PZT 1 (front)

b) RMSD, PZT 2 (back)

c) CCDM, PZT 1 (front)

b) CCDM, PZT 2 (back)

Source: Prepared by the author.

4.2.6 Correlation between EMI signatures and R_a parameter

Correlations between the average roughness (R_a parameter) and damage indices are presented in Figure 29. The Pearson coefficient points out better correlations for the CCDM index in general, as shown in Figure 29(b) and in Figure 29(d), than the correlations for the RMSD index, shown in Figure 29(a) and in Figure 29(c). The closer the coefficient to 1 or -1, the greater the correlation between the parameters. In contrast, the closer the coefficient to 0, the smaller is the correlation. Positive coefficients indicate that data are directly proportional, and, consequently, negative coefficients point to inversely proportional data.

Figure 29 – Correlation between average roughness and damage indices in the cylindrical grinding process

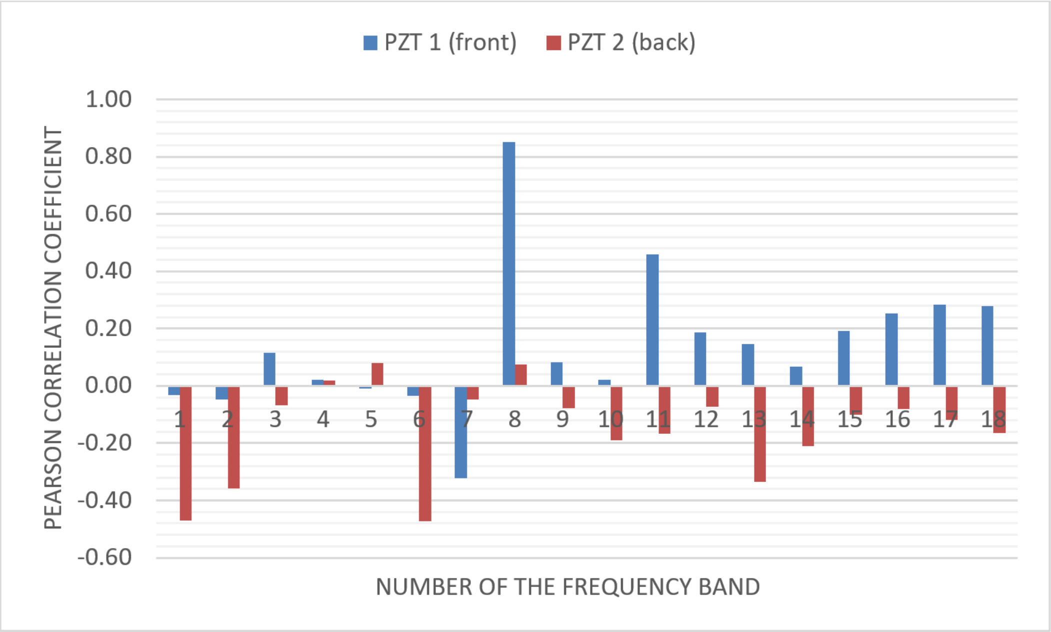

a) RMSD index for bandwidth of 10 kHz

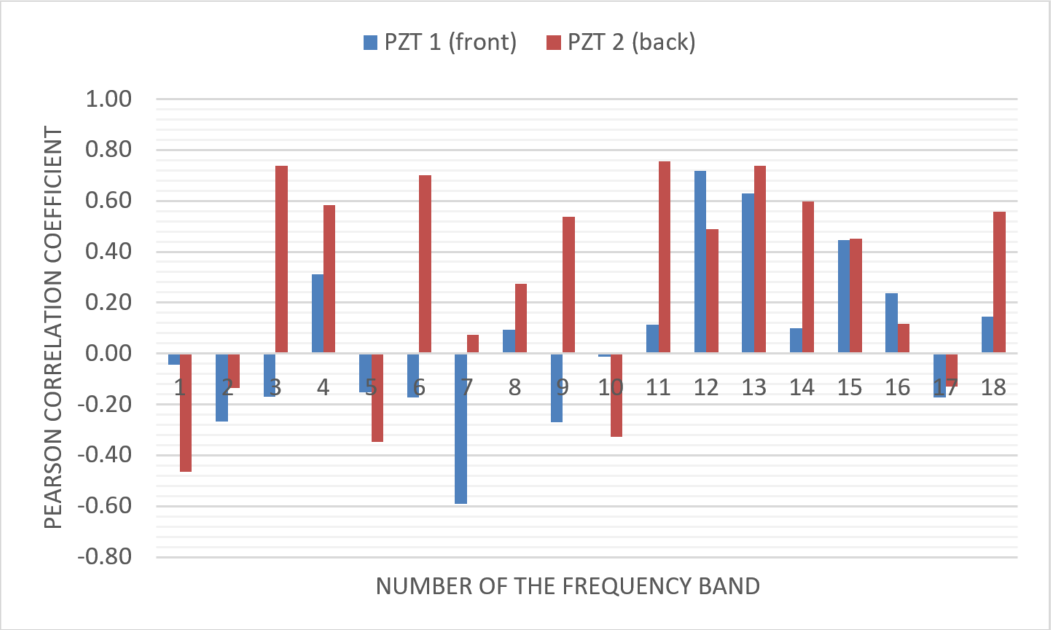

b) CCDM index for bandwidth of 10 kHz

Figure 29 – cont.

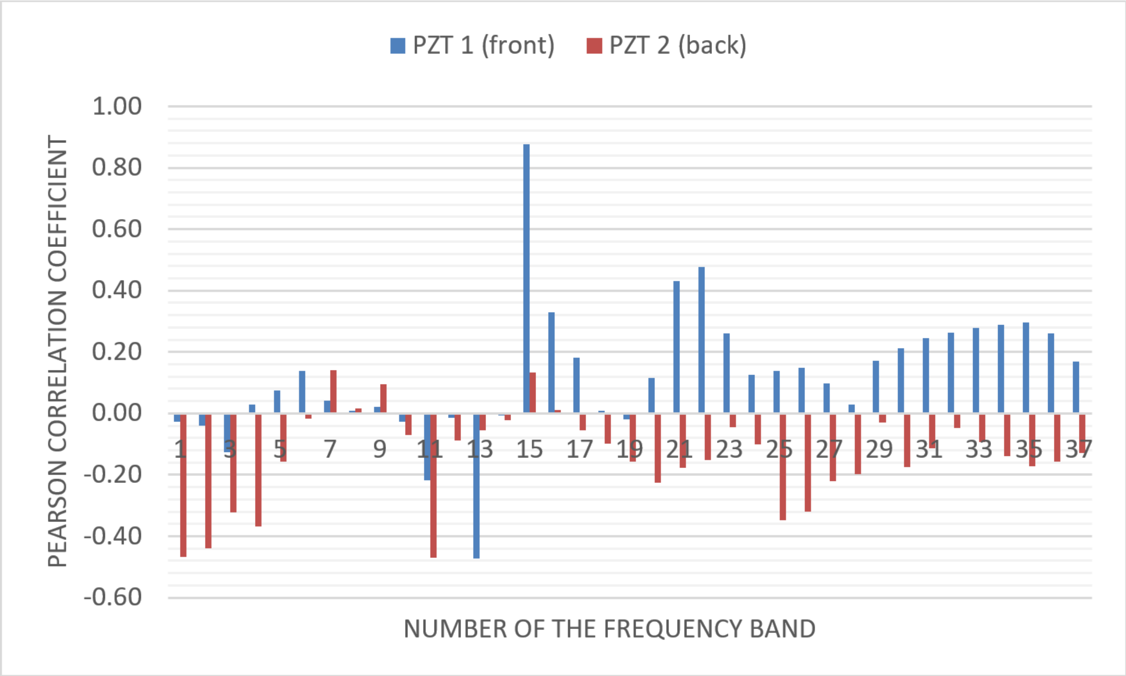

c) RMSD index for bandwidth of 5 kHz

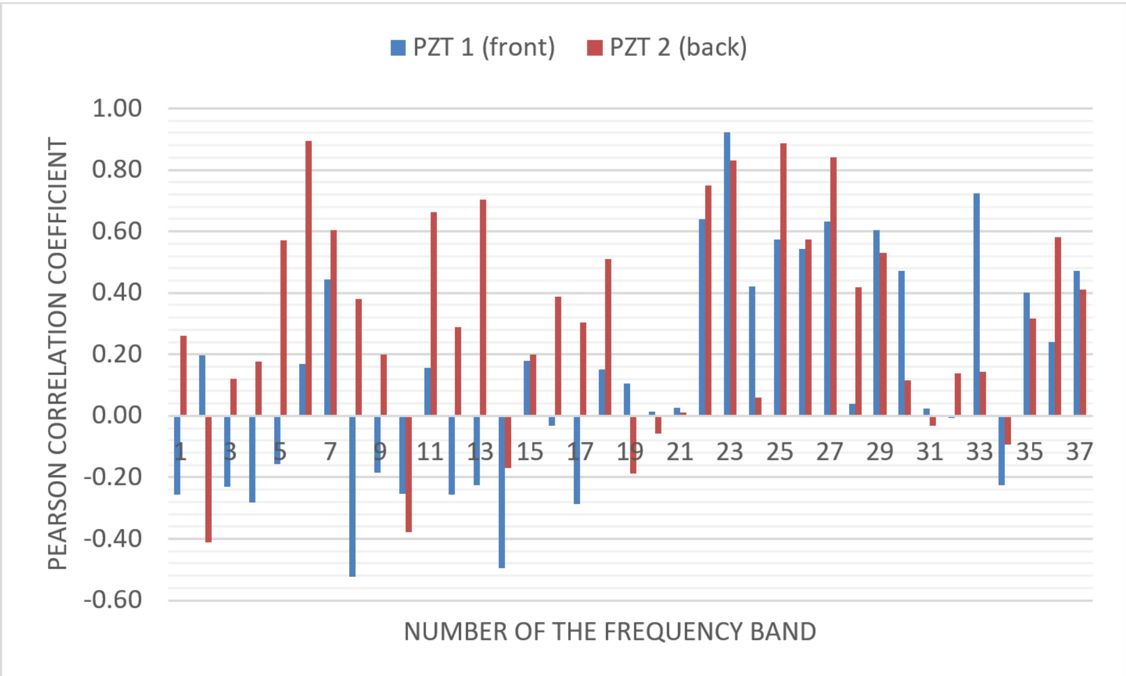

d) CCDM index for bandwidth of 5 kHz

Source: Prepared by the author.

Requirements for selection of the best frequency band that correlates average roughness with damage indices, besides choosing the furthest coefficient values from zero, are that coefficients for PZT 1 and for PZT 2 need to have the same signal; both are either positive or negative. Opposite signals for the same frequency band indicate that no repeatability was observed and, therefore, a structural monitoring system can provide different results for each measurement.

From Figure 29(a) and Figure 29(c), one notes that no good correlation was found for the RMSD index. Despite some good correlations that can be seen for some frequency bands, they did not occur for both PZT at the same time, which do not guarantee consistent results for the measurements. On the other hand, considering correlation coefficients above 0.60, CCDM index presented good correlations for both PZTs in some frequency bands, as follows:

- #13 (bw 10 kHz), shown in Figure 29(b),
- #22 (bw 5 kHz), shown in Figure 29(d),
- #23 (bw 5 kHz), shown in Figure 29(d),
- #27 (bw 5 kHz). shown in Figure 29(d).

These results show that the RMSD index (Figure 29(a) and in Figure 29(c)) is not a good statistical parameter to be employed in this specific application because sequential impedance measurements (PZT 1 and PZT 2) provided different distances between the baseline and damaged condition. In previous works, the RMSD index was efficient to quantify wear (Marchi *et al.*, 2015) and to correlate R_a with the EMI (Ferreira *et al.*, 2019) in surface grinding of ABNT N2711 steel. However, the present work verified that it is not efficient in cylindrical grinding of AISI – SAE 4340 steel. If correlation coefficients from PZT 1 and PZT 2 differs from each other in Figure 29, the respective signatures vary differently in amplitude, which is quantified by the RMSD index. One of the causes for the amplitude variation is temperature changes. Previous works stated that temperature variations change amplitude of impedance signatures. Baptista *et al.* (2014), verified that the lower the temperature is, the higher the electromechanical impedance indices values are. However, in the present work, temperature was kept constant during the measurements and EMI for both PZTs is collected practically simultaneous. Therefore, the RMSD index was affected by other factors which, after the grinding process, caused different variations for each PZT. Some hypotheses to consider include different distances from the sensor to the damaged layer, coupling variations, difference in sensitivity, and variation in workpiece positioning, etc.

On the other hand, from Figure 29(b) and in Figure 29(d), one notes that the CCDM index was shown to be less sensitive to those variations and presented better correlations between the parameters. In fact, monitoring systems that are employed in the field must be insulated from interferences to ensure effectiveness of measurements. The best correlation that was found between EMI and average roughness was CCDM frequency band #23 (bw 5 kHz), as shown in Figure 30 (a) and (b).

Figure 30 – Correlation between CCDM index and average roughness for the frequency band #23 (bw 5 kHz) in the cylindrical grinding process

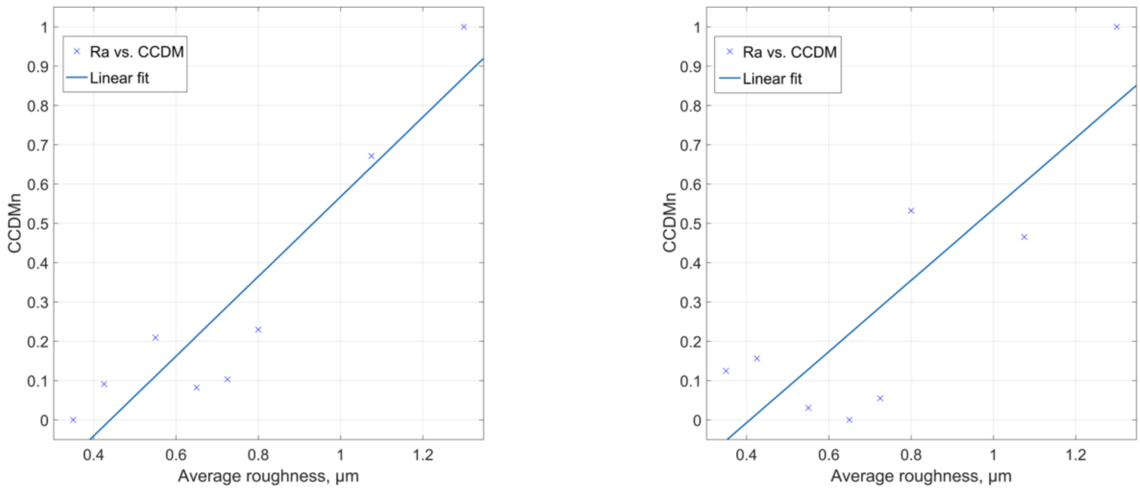

a) PZT 1 (front) b) PZT 2 (back)

Source: Prepared by the author.

From Figure 30 can be observed a linear tendency obtained for both PZTs. The higher the value of the average roughness is, the higher the values of the CCDMn index is as well, where CCDMn is the CCDM index linearly normalized (adjusted into the interval [0;1]). The correlation coefficient calculated for the average roughness and CCDMn index in the frequency band #23 (bw 5 kHz), that is 125-130 kHz, was 0.92 for the PZT 1 and 0.83 for the PZT 2. Also, the RMSE was 0.0384 for the PZT 1 and 0.1071 for the PZT 2.

5 CONCLUSIONS

In this work, the monitoring features applied to surface grinding and cylindrical plunge grinding were investigated independently. Some parameters to assess the surface integrity of workpieces and process efficiency were measured and some correlations were found with EMI measurements. The following conclusions can be drawn:

Surface grinding

- Severity of the process was correlated to damage indices and directly proportional relationships were preferable because it was adopted the hypothesis of that the greater the severity of the process, the greater the influence on the workpiece. So, the CCDM index calculated on the real part of the signatures for the frequency band of 70-75 kHz presented the best correlation with the equivalent chip thickness (h_{eq}) of the process. Such combination (CCDM real part 70-75 kHz) showed effective conditions because the same correlation was found for the parameters *ae* and v_w individually.
- Good correlations were found between h_{eq} and power, and between h_{eq} and roughness. No correlation was found between h_{eq} and microhardness.
- The best correlation between EMI measurements and power was found for the RMSD index for the real part of the impedance in the frequency band of 80-85 kHz, but this correlation requires further studies.
- The best correlation between EMI measurements and roughness was for the RMSD index for the real part of the impedance in the frequency band of 80-85 kHz. This configuration could be used to infer workpiece quality through indirect monitoring.
- The best correlation between EMI measurements and microhardness was found for the CCDM index for the imaginary part of the impedance in the frequency band range of 50-55 kHz.
- EMI technique is a good alternative to monitor surface grinding instead of using conventional techniques and has the advantage of employing low-cost PTZ diaphragms.

Cylindrical plunge grinding

- R_a roughness values increased with feed rate and workspeed, but with lesser influence of the latter. All the surface roughness values were below the upper reference limit for the grinding process, R_a = 1.6 µm.
- The surface roughness presented a correlation coefficient of 0.92 with the grinding power and noted that grinding power varied according to the severity of grinding.
- In the EMI measurements, the PZTs attached to a same sample showed differences between their signatures. The differences were quantified by the RMSD and CCDM indices calculated for the real part of the impedance, which presented a consistent result only for the CCDM index.
- Correlation between surface roughness and damage indices was studied and the best correlation was found to be with the CCDM index in the frequency band of 125-130 kHz, which resulted in a correlation coefficient of 0.92 for the PZT 1 and 0.83 for the PZT 2, respectively. That is a satisfactory result, considering that the PZT diaphragm costs less than 1 dollar while traditional monitoring systems, such as power and acoustic emission systems use very expensive equipment. These results can be improved by investigating different frequency bands with different bandwidths, or by studying other signal processing approaches for the EMI technique.

At the end, this work presented two different approaches, in which the EMI technique has been applied. For surface grinding, the RMSD index presented to be efficient to correlate EMI with power and average roughness, while the CCDM index showed efficiency to correlate EMI with equivalent chip thickness and microhardness. Frequencies from 50 kHz to 85 kHz showed to be promising to monitor the process. On the other hand, when performing cylindrical grinding, the CCDM index showed to be efficient to correlate EMI with average roughness. In this process, frequencies showed to be more promising around 135 kHz. Based on this difference, it is possible to presume that the EMI technique varies according to several features of the process, such as grinding wheel, workpiece size, steel type, etc. Therefore, monitoring based on electromechanical impedance must be individually adjusted for each application.

REFERENCES

4340 ALLOY BAR (no date) *TW Metals*. Available at: https://www.twmetals.com/products/bars/alloy-bar/4340-alloy-bar.html (Accessed: 3 July 2020).

Aguiar, P. R., Bianchi, E. C. and Canarim, R. C. (2012) 'Monitoring of Grinding Burn by Acoustic Emission', in *InTech*. Dr. Wojcie. Rijeka, Croatia, pp. 341–364. doi: 10.5772/31339.

Aguiar, P. R. de, Dotto, F. R. L. and Bianchi, E. C. (2005) 'Study of Thresholds to Burning in Surface Grinding Process', *Journal of the Brazilian Society of Mechanical Sciences and Engineering*, XXVII(2), pp. 150–156. doi: 10.1590/S1678-58782005000200007.

Akbari, M. *et al.* (2016) 'A new value for Johnson Cook damage limit criterion in machining with large negative rake angle as basis for understanding of grinding', *Journal of Materials Processing Tech.* Elsevier B.V., 234, pp. 58–71. doi: 10.1016/j.jmatprotec.2016.03.009.

Alexandre, F. A. F. A. *et al.* (2018) 'Tool Condition Monitoring of Aluminum Oxide Grinding Wheel using AE and Fuzzy Model', *The International Journal of Advanced Manufacturing Technology*. The International Journal of Advanced Manufacturing Technology, 1(1), pp. 1–13. doi: 10.1007/s00170-018-1582-0.

Alhadeff, L. L. *et al.* (2019) 'Protocol for tool wear measurement in micro-milling', *Wear*. Elsevier B.V., 420–421(December 2018), pp. 54–67. doi: 10.1016/j.wear.2018.11.018.

Arun, A. *et al.* (2018) 'Tool Condition Monitoring of Cylindrical Grinding Process Using Acoustic Emission Sensor', *Materials Today: Proceedings*. Elsevier Ltd, 5(5), pp. 11888–11899. doi: 10.1016/j.matpr.2018.02.162.

Asiltürk, I. and Çunkaş, M. (2011) 'Modeling and prediction of surface roughness in turning operations using artificial neural network and multiple regression method', *Expert Systems with Applications*, 38(5), pp. 5826–5832. doi: 10.1016/j.eswa.2010.11.041.

AZoM (2012) *AISI 4340 Alloy Steel (UNS G43400)*, *AZO Materials*. Available at: https://www.azom.com/article.aspx?ArticleID=6772 (Accessed: 5 July 2020).

Balsamo, V. *et al.* (2016) 'Multi Sensor Signal Processing for Catastrophic Tool Failure Detection in Turning', *Procedia CIRP*. Elsevier B.V., 41, pp. 939–944. doi: 10.1016/j.procir.2016.01.010.

Baptista, F. *et al.* (2014) 'An Experimental Study on the Effect of Temperature on Piezoelectric Sensors for Impedance-Based Structural Health Monitoring', *Sensors*, 14(1), pp. 1208–1227. doi: 10.3390/s140101208.

Baptista, F. G. *et al.* (2013) 'An experimental study on the effect of temperature on piezoelectric sensors for impedance-based structural health monitoring', *Sensors*, 14, pp. 1208–1227. doi: 10.3390/s140101208.

Baptista, F. G. and Filho, J. V. (2009) 'A new impedance measurement system for PZT-based structural health monitoring', *IEEE Trans. Instrum. Meas*, 58(10), pp. 3602–3608. doi: 10.1109/TIM.2009.2018693.

Baptista, F. G. and Filho, J. V. (2011) ‘Piezoelectric Transducers Applied in Structural Health Monitoring: Data Acquisition and Virtual Instrumentation for Electromechanical Impedance Technique’, in *InTech*. Dr. Farzad, pp. 105–128. doi: 10.5772/28313.

Baptista, F. G., Filho, J. V. and Inman, D. J. (2010) ‘Influence of excitation signal on impedance-based structural health monitoring’, *Journal of Intelligent Material Systems and Structures*, 21(14), pp. 1409–1416. doi: 10.1177/1045389X10385032.

Baptista, F. G., Filho, J. V. and Inman, D. J. (2012) ‘Real-time multi-sensors measurement system with temperature effects compensation for impedance-based structural health monitoring’, *Structural Health Monitoring*, 11(2), pp. 173–186. doi: 10.1177/1475921711414234.

Batista da Silva, R. *et al.* (2018) ‘Electromechanical impedance (EMI) technique as alternative to monitor workpiece surface damages after the grinding operation’, *International Journal of Advanced Manufacturing Technology*. The International Journal of Advanced Manufacturing Technology, 98(9–12), pp. 2429–2438. doi: 10.1007/s00170-018-2390-2.

Baumgart, C., Heizer, V. and Wegener, K. (2018) ‘In-process workpiece based temperature measurement in cylindrical grinding’, *Procedia CIRP*. Elsevier B.V., 77(Hpc), pp. 42–45. doi: 10.1016/j.procir.2018.08.206.

Bhuiyan, M. S. H. *et al.* (2016) ‘Application of acoustic emission sensor to investigate the frequency of tool wear and plastic deformation in tool condition monitoring’, *Measurement*. Elsevier Ltd, 92, pp. 208–217. doi: 10.1016/j.measurement.2016.06.006.

Bianchi, E. C. *et al.* (1996) ‘Análise do Comportamento de Rebolos Convencionais na Retificação de Aços Dúcteis’, in. Recife - PE: IV CONGRESSO NORTE NORDESTE DE ENGENHARIA MECÂNICA, pp. 387–392.

Boaron, A. and Weingaertner, W. L. (2018) ‘Dynamic in-process characterization method based on acoustic emission for topographic assessment of conventional grinding wheels’, *Wear*. Elsevier B.V., 406–407(April), pp. 218–229. doi: 10.1016/j.wear.2018.04.009.

Budoya, D. E. and Baptista, F. G. (2018) ‘A Comparative Study of Impedance Measurement Techniques for Structural Health Monitoring Applications’, *IEEE Transactions on Instrumentation and Measurement*, 67(4), pp. 912–924. doi: 10.1109/TIM.2018.2792854.

Caggiano, A. *et al.* (2018) ‘Dimensionality Reduction of Sensorial Features by Principal Component Analysis for ANN Machine Learning in Tool Condition Monitoring of CFRP Drilling’, *Procedia CIRP*. Elsevier B.V., 78, pp. 307–312. doi: 10.1016/j.procir.2018.09.072.

Campeiro, L. M., da Silveira, R. Z. M. and Baptista, F. G. (2018) ‘Impedance-based damage detection under noise and vibration effects’, *Structural Health Monitoring*, 17(3), pp. 654–667. doi: 10.1177/1475921717715240.

Castro, B. *et al.* (2016) ‘Partial Discharge Monitoring in Power Transformers Using Low-Cost Piezoelectric Sensors’, *Sensors*, 16(8), p. 1266. doi: 10.3390/s16081266.

Cearsolo, X. *et al.* (2016) ‘Dry-dressing for ecological grinding’, *Journal of Cleaner Production*, 135, pp. 633–643. doi: 10.1016/j.jclepro.2016.06.117.

da Conceição Junior, P. O. *et al.* (2018) ‘Time-domain Analysis Based on the Electromechanical Impedance Method for Monitoring of the Dressing Operation’, *Procedia CIRP*. The Author(s), 67(July 2017), pp. 319–324. doi: 10.1016/j.procir.2017.12.220.

Da Conceição Junior, P. O. *et al.* (2018) ‘Time-domain Analysis Based on the Electromechanical Impedance Method for Monitoring of the Dressing Operation’, in *Procedia CIRP*. doi: 10.1016/j.procir.2017.12.220.

D’Addona, D. M. *et al.* (2016) ‘Neural Networks Tool Condition Monitoring in Single-point Dressing Operations’, *Procedia CIRP*. Elsevier B.V., 41, pp. 431–436. doi: 10.1016/j.procir.2016.01.001.

Dai, Y. and Zhu, K. (2018) ‘A machine vision system for micro-milling tool condition monitoring’, *Precision Engineering*. Elsevier, 52(May 2017), pp. 183–191. doi: 10.1016/j.precisioneng.2017.12.006.

Dias, E. A. *et al.* (2016) ‘Monitoring of through-feed centreless grinding processes with acoustic emission signals’, *Measurement*, 94, pp. 71–79. doi: 10.1016/j.measurement.2016.07.075.

DINIZ, A. E., MARCONDES, F. C. and COPPINI, N. L. (2010) *Tecnologia da usinagem dos materiais*. 4th edn. Campinas: Artiliber Editora Ltda.

Dong Wang, G. *et al.* (2019) ‘Monitoring the drilling process of GFRP laminates with carbon nanotube buckypaper sensor’, *Composite Structures*. Elsevier, 208(September 2018), pp. 114–126. doi: 10.1016/j.compstruct.2018.10.016.

Drazumeric, R., Badger, J. and Krajnik, P. (2014) ‘Geometric, kinematical and thermal analyses of non-round cylindrical grinding’, *Journal of Materials Processing Technology*. Elsevier B.V., 214(4), pp. 818–827. doi: 10.1016/j.jmatprotec.2013.12.007.

Drouillet, C. *et al.* (2016) ‘Tool life predictions in milling using spindle power with the neural network technique’, *Journal of Manufacturing Processes*. The Society of Manufacturing Engineers, 22, pp. 161–168. doi: 10.1016/j.jmapro.2016.03.010.

Fávero, L. P. and Belfiore, P. (2017) *Manual de Análise de Dados ESTATÍSTICA MODELAGEM MULTIVARIADA COM EXCEL, SPSS E STATA*, *Elsevier*. doi: 10.1017/CBO9781107415324.004.

Ferreira, F. I. *et al.* (2018) ‘Inferential measurement of the dresser width for the grinding process automation’, *The International Journal of Advanced Manufacturing Technology*. The International Journal of Advanced Manufacturing Technology, 100(9–12), pp. 1–12. doi: 10.1007/s00170-018-2869-x.

Ferreira, F. I. F. I. *et al.* (2019) ‘Electromechanical impedance (EMI) measurements to infer features from the grinding process’, *The International Journal of Advanced Manufacturing Technology*. doi: 10.1007/s00170-019-04733-8.

De Freitas, E. S. *et al.* (2017) ‘Equivalent Circuit of Piezoelectric Diaphragms for Impedance-Based Structural Health Monitoring Applications’, *IEEE Sensors Journal*, 17(17), pp. 5537–5546. doi: 10.1109/JSEN.2017.2725946.

GRAF, W. (2004) *Cylindrical Grinding*. WST Winterthur Schleiftechnik AG.

Grote, A. (2019) *Springer Handbook of Mechanical Engineering*. 1st edn. Edited by E. K. Grote, Karl-Heinrich, Antonsson. New York: Springer.

Hase, A. *et al.* (2014) 'The relationship between acoustic emission signals and cutting phenomena in turning process', *International Journal of Advanced Manufacturing Technology*, 70(5–8), pp. 947–955. doi: 10.1007/s00170-013-5335-9.

Hassui, A. and Diniz, A. E. (2003) 'Correlating surface roughness and vibration on plunge cylindrical grinding of steel', *International Journal of Machine Tools & Manufacture*, 43, pp. 855–862. doi: 10.1016/S0890-6955(03)00049-X.

He, B. *et al.* (2019) 'A survey of methods for detecting metallic grinding burn', *Measurement: Journal of the International Measurement Confederation*. Elsevier Ltd, 134, pp. 426–439. doi: 10.1016/j.measurement.2018.10.093.

Hesser, D. F. and Markert, B. (2019) 'Tool wear monitoring of a retrofitted CNC milling machine using artificial neural networks', *Manufacturing Letters*. Society of Manufacturing Engineers (SME), 19, pp. 1–4. doi: 10.1016/j.mfglet.2018.11.001.

Hocheng, H. *et al.* (2018) 'Tool wear monitoring in single-point diamond turning using laser scattering from machined workpiece', *Journal of Manufacturing Processes*. The Society of Manufacturing Engineers, 31, pp. 405–415. doi: 10.1016/j.jmapro.2017.12.007.

Junior, P., D'addona, D. M., *et al.* (2018) 'Dressing tool condition monitoring through impedance-based sensors: Part 1—pzt diaphragm transducer response and emi sensing technique', *Sensors (Switzerland)*, 18(12). doi: 10.3390/s18124455.

Junior, P., D'Addona, D. M., *et al.* (2018) 'Dressing tool condition monitoring through impedance-based sensors: Part 2—neural networks and K-nearest neighbor classifier approach', *Sensors (Switzerland)*, 18(12). doi: 10.3390/s18124453.

KING, R. I. and HAHN, R. S. (1992) *Handbook of Modern Grinding Technology*. 3rd edn. New York.

Klaic, M. *et al.* (2018) 'Tool wear monitoring in rock drilling applications using vibration signals', *Wear*. Elsevier B.V., 408–409(January), pp. 222–227. doi: 10.1016/j.wear.2018.05.012.

Klaic, M., Staroveski, T. and Udiljak, T. (2014) 'Tool wear classification using decision treesin stone drilling applications: A preliminary study', *Procedia Engineering*. Elsevier B.V., 69, pp. 1326–1335. doi: 10.1016/j.proeng.2014.03.125.

Linke, B. (2008) 'Dressing process model for vitrified bonded grinding wheels', *CIRP Annals - Manufacturing Technology*, 57(1), pp. 345–348. doi: 10.1016/j.cirp.2008.03.083.

Macedo, C. V. (2012) *Análise da Influência dos Parâmetros de Retificação Cilíndrica na Rugosidade Média (Ra) da Luva Externa Para Cardan*. Universidade Federal do Rio Grande do Sul.

Malkin, S. and Guo, C. (2007) 'Thermal Analysis of Grinding', *CIRP Annals - Manufacturing Technology*, 56(2), pp. 760–782. doi: 10.1016/j.cirp.2007.10.005.

Malkin, S. and Guo, C. (2008) *Grinding Technology: Theory and Applications of Machining with Abrasives*. 2ª ed. New York: Industrial Press Inc.

Marchi, M. *et al.* (2015) 'Grinding process monitoring based on electromechanical impedance measurements', *Measurement Science and Technology*. IOP Publishing, 26(4), p. 045601. doi: 10.1088/0957-0233/26/4/045601.

Marinescu, I. D. *et al.* (2007) *Handbook of Machining with Grinding Wheels*. 1st edn. New York: CRC Press.

Martins, C. H. R. *et al.* (2014) 'Tool condition monitoring of single-point dresser using acoustic emission and neural networks models', *IEEE Transactions on Instrumentation and Measurement*, 63(3), pp. 667–679. doi: 10.1109/TIM.2013.2281576.

Miranda, H. I. *et al.* (2015) 'Monitoring single-point dressers using fuzzy models', in *9th CIRP Conference on Intelligent Computation in Manufacturing Engineering*. Elsevier B.V., pp. 281–286. doi: 10.1016/j.procir.2015.06.050.

Moia, D. F. G. *et al.* (2015) 'Tool condition monitoring of aluminum oxide grinding wheel in dressing operation using acoustic emission and neural networks', *Journal of the Brazilian Society of Mechanical Sciences and Engineering*, 63(3), pp. 627–640. doi: 10.1007/s40430-014-0191-6.

Molaie, M. M., Akbari, J. and Movahhedy, M. R. (2016) 'Ultrasonic assisted grinding process with minimum quantity lubrication using oil-based nanofluids', *Journal of Cleaner Production*. Elsevier Ltd, 129, pp. 212–222. doi: http://dx.doi.org/10.1016/j.jclepro.2016.04.080.

Na, S. and Lee, H. K. (2013) 'A multi-sensing electromechanical impedance method for non-destructive evaluation of metallic structures', *Smart Materials and Structures*, 22(9), p. 8pp. doi: 10.1088/0964-1726/22/9/095011.

Na, W. S. and Baek, J. (2018) 'A review of the piezoelectric electromechanical impedance based structural health monitoring technique for engineering structures', *Sensors (Switzerland)*, 18(5). doi: 10.3390/s18051307.

Neslušan, M. *et al.* (2017) 'Monitoring of grinding burn via Barkhausen noise emission in case-hardened steel in large-bearing production', *Journal of Materials Processing Technology*, pp. 104–117. doi: 10.1016/j.jmatprotec.2016.09.015.

Neto, R. F. G. *et al.* (2014) 'Monitoring of Grinding Burn by AE and Vibration Signals', *Proceedings of the 6th International Conference on Agents and Artificial Intelligence*. SCITEPRESS - Science and and Technology Publications, pp. 272–279. doi: 10.5220/0004753602720279.

Nguyen, D. T. *et al.* (2019) 'Online monitoring of surface roughness and grinding wheel wear when grinding Ti-6Al-4V titanium alloy using ANFIS-GPR hybrid algorithm and Taguchi analysis', *Precision Engineering*. Elsevier, 55(October 2018), pp. 275–292. doi: 10.1016/j.precisioneng.2018.09.018.

Oliveira, J. F. G. *et al.* (2009) 'Industrial challenges in grinding', *CIRP Annals - Manufacturing Technology*, 58(2), pp. 663–680. doi: 10.1016/j.cirp.2009.09.006.

Park, G. *et al.* (2003) 'Overview of piezoelectric impedance-based health monitoring and path forward', *Shock and Vibration Digest*, 35(6), pp. 451–463. doi: 10.1177/05831024030356001.

Patra, K. *et al.* (2017) 'Artificial neural network based tool condition monitoring in micro mechanical peck drilling using thrust force signals', *Precision Engineering*. Elsevier Inc., 48, pp. 279–291. doi: 10.1016/j.precisioneng.2016.12.011.

Sahni, Y., Cao, J. and Liu, X. (2018) 'MidSHM: A Middleware for WSN-based SHM Application using Service-Oriented Architecture', *Future Generation Computer Systems*. Elsevier B.V., 80, pp. 263–274. doi: 10.1016/j.future.2017.01.022.

Sarikaya, M. and Gullu, A. (2014) 'Taguchi design and response surface methodology based analysis of machining parameters in CNC turning under MQL', *Journal of Cleaner Production*, 65, pp. 604–616. doi: 10.1016/j.jclepro.2013.08.040.

Scheffer, C. *et al.* (2003) 'Development of a tool wear-monitoring system for hard turning', *International Journal of Machine Tools and Manufacture*, 43(10), pp. 973–985. doi: 10.1016/S0890-6955(03)00110-X.

Silva De Freitas, E. and Guimarães Baptista, F. (2016) 'Experimental analysis of the feasibility of low-cost piezoelectric diaphragms in impedance-based SHM applications', *Sensors and Actuators, A: Physical*. Elsevier B.V., 238, pp. 220–228. doi: 10.1016/j.sna.2015.11.031.

da Silveira, R. Z. M., Campeiro, L. M. and Baptista, F. G. (2017) 'Performance of three transducer mounting methods in impedance-based structural health monitoring applications', *Journal of Intelligent Material Systems and Structures*, p. 1045389X1768994. doi: 10.1177/1045389X17689942.

Sinha, M. K. *et al.* (2016) 'An investigation on surface burn during grinding of Inconel 718', *Journal of Manufacturing Processes*. The Society of Manufacturing Engineers, 21, pp. 124–133. doi: 10.1016/j.jmapro.2015.12.004.

Tanaka, K. and Koshy, P. (2018) 'A pneumatic sensor for grinding wheel condition monitoring', *Precision Engineering*. Elsevier Inc. doi: 10.1016/j.precisioneng.2018.09.005.

Teti, R. *et al.* (2010) 'Advanced monitoring of machining operations', *CIRP Annals - Manufacturing Technology*, 59, pp. 717–739. doi: 10.1016/j.cirp.2010.05.010.

Thanedar, A. *et al.* (2017) 'Surface integrity investigation including grinding burns using barkhausen noise (BNA)', *Journal of Manufacturing Processes*. The Society of Manufacturing Engineers, 30, pp. 226–240. doi: 10.1016/j.jmapro.2017.09.026.

Tinoco, H. A. *et al.* (2019) 'Evaluation of a Piezo-actuated sensor for monitoring elastic variations of its support with impedance-based measurements', *Sensors (Switzerland)*, 19(1). doi: 10.3390/s19010184.

Tuan, A. and Lee, D. (2008) 'Correlation of grinding wheel topography and grinding performance : A study from a viewpoint of three-dimensional surface characterisation', *Journal of Materials Processing Technology*, 8(1995), pp. 14–23. doi: 10.1016/j.jmatprotec.2007.12.128.

Uekita, M. and Takaya, Y. (2017) 'Tool condition monitoring technique for deep-hole drilling of large components based on chatter identification in time –

frequency domain', *Measurement*. Elsevier Ltd, 103, pp. 199–207. doi: 10.1016/j.measurement.2017.02.035.

Vendrame, S. *et al.* (2018) 'Surface integrity assessment of M3 HSS cutting taps after grinding at various machining conditions', *International Journal of Advanced Manufacturing Technology*. The International Journal of Advanced Manufacturing Technology, 98(1–4), pp. 617–627. doi: 10.1007/s00170-018-2245-x.

Vieira Filho, J., Baptista, F. G. and Inman, D. J. (2011) 'Time-domain analysis of piezoelectric impedance-based structural health monitoring using multilevel wavelet decomposition', *Mechanical Systems and Signal Processing*, 25(5), pp. 1550–1558. doi: 10.1016/j.ymssp.2010.12.003.

'Villares Metals. Plastic mold steel - N2711M grade' (2017).

Wang, Y. *et al.* (2016) 'Experimental evaluation of the lubrication properties of the wheel / workpiece interface in MQL grinding with different nanofluids', *Tribiology International*. Elsevier, 99, pp. 198–210. doi: 10.1016/j.triboint.2016.03.023.

Wang, Z. *et al.* (2001) 'Neural network detection of grinding burn from acoustic emission', *International Journal of Machine Tools and Manufacture*, 41(2), pp. 283–309. doi: 10.1016/S0890-6955(00)00057-2.

Wegener, K. *et al.* (2011) 'Conditioning and monitoring of grinding wheels', *CIRP Annals - Manufacturing Technology*. CIRP, 60(2), pp. 757–777. doi: 10.1016/j.cirp.2011.05.003.

Yang, Z. *et al.* (2014) 'Application of Hilbert–Huang Transform to acoustic emission signal for burn feature extraction in surface grinding process', *Measurement*. Elsevier Ltd, 47, pp. 14–21. doi: 10.1016/j.measurement.2013.08.036.

Yang, Z. and Yu, Z. (2012) 'Grinding wheel wear monitoring based on wavelet analysis and support vector machine', *International Journal of Advanced Manufacturing Technology*, 62(1–4), pp. 107–121. doi: 10.1007/s00170-011-3797-1.

Yang, Z. and Yu, Z. (2013) 'Experimental study of burn classification and prediction using indirect method in surface grinding of AISI 1045 steel', *The International Journal of Advanced Manufacturing Technology*, 68(9–12), pp. 2439–2449. doi: 10.1007/s00170-013-4882-4.

Zhang, X. Y. *et al.* (2018) 'A multi-sensor based online tool condition monitoring system for milling process', *Procedia CIRP*, 72, pp. 1136–1141. doi: 10.1016/j.procir.2018.03.092.